Neurobiology of Disease 121 (2019) 106–119

Contents lists available at ScienceDirect

Neurobiology of Disease

journal homepage: www.elsevier.com/locate/ynbdi

Ultra-micronized palmitoylethanolamide rescues the cognitive decline-associated loss of neural plasticity in the neuropathic mouse entorhinal cortex-dentate gyrus pathway

Serena Boccella[a,1], Claudia Cristiano[b,1], Rosaria Romano[a], Monica Iannotta[a], Carmela Belardo[a], Antonio Farina[a], Francesca Guida[a], Fabiana Piscitelli[c], Enza Palazzo[a], Mariacristina Mazzitelli[d], Roberta Imperatore[e], Lea Tunisi[c], Vito de Novellis[a], Luigia Cristino[c], Vincenzo Di Marzo[c], Antonio Calignano[b], Sabatino Maione[a], Livio Luongo[a,*]

[a] Department of Experimental Medicine, Pharmacology Division, University of Campania "L. Vanvitelli", 80138 Naples, Italy
[b] Department of Pharmacy, School of Medicine, University of Naples Federico II, Naples, Italy
[c] Endocannabinoid Research Group, Institute of Biomolecular Chemistry, CNR, Pozzuoli, Italy
[d] Department of Pharmacology and Neuroscience, Texas Tech University Health Sciences Center, Lubbock, TX
[e] Department of Science and Technology, University of Sannio, Benevento, Italy

ARTICLE INFO

Keywords:
Spared nerve injury
pamitoylethanolamide
long term potentiation
PPARα
cognitive performance
synaptogenesis

ABSTRACT

Chronic pain is associated with cognitive deficits. Palmitoylethanolamide (PEA) has been shown to ameliorate pain and pain-related cognitive impairments by restoring glutamatergic synapses functioning in the spared nerve injury (SNI) of the sciatic nerve in mice. SNI reduced mechanical and thermal threshold, spatial memory and LTP at the lateral entorhinal cortex (LEC)-dentate gyrus (DG) pathway. It decreased also postsynaptic density, volume and dendrite arborization of DG and increased the expression of metabotropic glutamate receptor 1 and 7 (mGluR1 and mGluR7), of the GluR1, GluR1s845 and GluR1s831 subunits of AMPA receptor and the levels of glutamate in the DG. The level of the endocannabinoid 2-arachidonoylglycerol (2-AG) was instead increased in the LEC. Chronic treatment with PEA, starting from when neuropathic pain was fully developed, was able to reverse mechanical allodynia and thermal hyperalgesia, memory deficit and LTP in SNI wild type, but not in PPARα null, mice. PEA also restored the level of glutamate and the expression of phosphorylated GluR1 subunits, postsynaptic density and neurogenesis. Altogether, these results suggest that neuropathic pain negatively affects cognitive behavior and related LTP, glutamatergic synapse and synaptogenesis in the DG. In these conditions PEA treatment alleviates pain and cognitive impairment by restoring LTP and synaptic maladaptative changes in the LEC-DG pathway. These outcomes open new perspectives for the use of the N-acylethanolamines, such as PEA, for the treatment of neuropathic pain and its central behavioural sequelae.

1. Introduction

In the last two decades most of studies on chronic pain-related synaptic plasticity changes underlying cognitive/affective consequences (Kuner, 2015; Moriarty et al., 2016) have been focused on cortical (Giordano et al., 2012; Gustin et al., 2012) and non-cortical supraspinal structures (Grilli, 2017; Thompson & Neugebauer, 2017). How, chronic pain influences the hippocampus (archicortex) is still little investigated (Gol & Faibish, 1966). The hippocampus belongs to the Papez circuit, a neural network that, by connecting the hypothalamus to the limbic areas, represents the anatomical substrate for emotional experiences involved in learning, memory and motivation (Seralynne, 2013). Persistent pain altered hippocampus neuron function (Ikonen & Riekkinen, 1999; Van der Staay et al., 2000) whereas neuropathic pain reduced synaptic plasticity (LTP or STP) at dentate gyrus (DG), CA1 or CA3 synapses (Kodama et al., 2007; Ren et al., 2011; Mutso et al., 2012), as well as DG neurogenesis (Dellarole et al., 2014) and activated mTOR pathways (Kwon et al., 2017). Much of the cortical information that arrives at the hippocampus enters through the entorhinal cortex, and much of the return projection to the neocortex arises from the

* Corresponding author.
E-mail address: livio.luongo@unicampania.it (L. Luongo).
[1] Co-first authors.

https://doi.org/10.1016/j.nbd.2018.09.023
Received 27 July 2018; Received in revised form 10 September 2018; Accepted 24 September 2018
Available online 25 September 2018
0969-9961/ Published by Elsevier Inc.

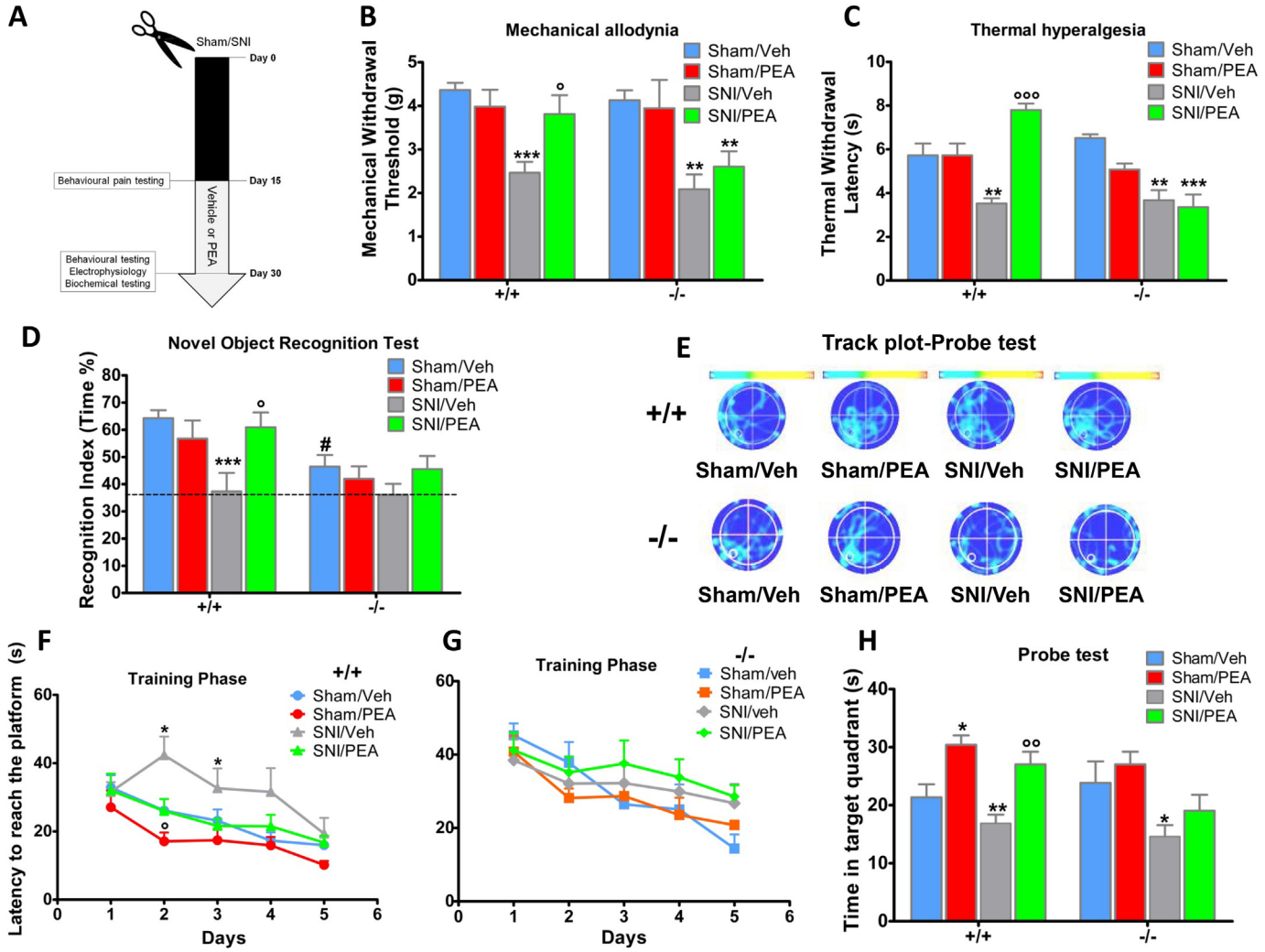

Fig. 1. Effect of vehicle or PEA on pain and cognitive behavior in sham and SNI WT (+/+) and PPARα null mice (-/-). "A" shows the experimental design and timeline of sham or SNI surgery and treatment with vehicle or PEA. "B", "C" and "D" show the effect of vehicle or PEA on mechanical withdrawal threshold (MWT), thermal withdrawal latency (TWL) and recognition index (RI) in sham or SNI WT and PPARα null mice. "E" shows the effect of vehicle or PEA on the occupancy plots in the Morris water maze (MWM) probe test in sham and SNI WT and PPARα null mice. "F" and "G" show the effect of vehicle or PEA on the latency to reach the platform in sham and SNI WT (F) and PPARα null mice (G) during 5 days of MWM training phase. "H" shows the effect of vehicle or PEA in the target quadrant in the MWM probe tests. Data are represented as mean ± SEM of MWT, TWL, RI, latency to reach the platform or the time spent in the target quadrant. * indicates significant differences *vs* sham/veh, ° indicate significant differences *vs* SNI/veh, # indicate significant differences *vs* sham/veh WT (+/+) mice (n = 6-7). $P < 0.05$ was considered statistically significant.

entorhinal cortex. Recent evidence has shown that the entorhinal cortex-hippocampus cross talk is critical in persistent pain and that cortical connections with the hippocampus can differently affect pain perception (Zhang et al., 2014; McKenna & Melzack, 2001). In particular, the interactions between the lateral entorhinal cortex (LEC) and the DG are involved in the integration of emotionally salient information associated with spatial-temporal orientation and place memorization (Bush et al., 2014). The glutamatergic (Glu) and the endocannabinoid (eCB) systems apart from being involved in neuropathic pain development (Guindon & Hohmann, 2009; Luongo et al., 2013; Palazzo et al., 2001), play an essential role on the generation of the long-term potentiation (LTP) in the lateral perforant path (LPP)-DG pathway (Wang et al., 2016, 2018). Among the endocannabinoids, palmitoylethanolamide (PEA) has shown to exert antinflammatory, analgesic, immunomodulatory and neuroprotective effects and to reverse cognitive impairments through the activation of peroxisome proliferator-activated receptor (PPAR)-α in several chronic pain conditions (Guida et al., 2015, 2017a, 2017b; Lo Verme et al., 2006). On this basis, the current study has first evaluated whether neuropathic pain-induced sensory and cognitive impairments are associated with neuroplasticity deficits, biochemical modifications in glutamatergic and endocannabinoid signaling and neuroanatomical alterations in the DG and then whether i) a chronic treatment with PEA could rescue these changes and ii) the effects of PEA were mediated by PPARα. For the chronic treatment with PEA the ultramicronized formulation (um-PEA) has been used, due to the higher solubility and bioavailability after systemic administration (Fusco et al., 2018)

2. Materials and methods

2.1. Animals

Male wild-type and *Ppar-α−/−* (*B6.129S4-SvJae-Pparatm1Gonz*) mice were generated in the laboratory of the Pharmacy Department of the University of Naples "Federico II", through backcrossing with *C57BL6* mice for 10 generations, and the colony was established and maintained by heterozygous crossing. Mice were genotyped as described on the supplier webpage (http://jaxmice.jax.org), with minor

modifications. However, based on the large number of experiments, also male C57BL/6J mice purchased by Envigo (Italy) were used as controls for other experiments, as no significant differences were observed in experimental responses between the two strains of animals. Wild type, C57 BL/6J and PPARα null mice, weighing 25-30 g were housed three per cage under controlled illumination (12 h light/dark cycle; light on 6:00 A.M.) and standard environmental conditions (ambient temperature 20–22°C, humidity 55–60%) for at least 1 week before the commencement of experiments. Mice chow and tap water were available ad libitum. The experimental procedures were approved by the Animal Ethics Committee of University of Campania "L. Vanvitelli" of Naples. Animal care was in compliance with Italian (D.L. 116/92) and European Commission (O.J. of E.C. L358/1 18/12/86) regulations on the protection of laboratory animals. All efforts were made to reduce both animal numbers and suffering during the experiments.

2.2. Spared nerve injury

Neuropathic pain was induced according to the method of Decosterd and Woolf (Decosterd & Woolf, 2000). Mice were anaesthetized with sodium pentobarbital (50 mg/kg, i.p.), the sciatic nerve was exposed at the level of its trifurcation and the tibial and common peroneal nerves were tightly ligated with 5.0 silk thread and then transected just distal to the ligation, leaving the sural nerve intact. Sham mice were anesthetized, the sciatic nerve was exposed at the same level, but not ligated.

2.3. Treatment

The chronic treatment with PEA (10 mg/kg, i.p. once a day) started 15 days after the sham or SNI surgery (day 0) and lasted for 15 days, based on the experimental protocol used in our previous studies (Guida et al., 2015, 2017a). Ultramicronized palmitoylethanolamide (um-PEA) has been provided by Epitech group Spa (Italy). Sham and SNI mice were used for all experiments 30 days after surgery. A schematic illustration showing the timeline of surgery and treatment in sham and SNI mice is shown in Fig. 1A.

2.4. Mechanical allodynia

Mechanical allodynia was evaluated in sham or SNI mice by the dynamic plantar aesthesiometer (Ugo Basile, Varese, Italy) as described by Guida et al. (2017a). Mice were allowed to freely move in 1 of the 2 compartments of the enclosure, positioned on the metal mesh surface, and allowed to habituate to the testing environment before any measurement was taken. After 30-minute habituation period, the mechanical stimulus, a steel rod (2 mm) pushed with ascending force (0-30 g in 10 seconds), was delivered to the plantar surface of the hind paw of the mouse from below the floor of the test chamber by an automated testing device. When the mouse withdrew its hind paw, the mechanical stimulus was automatically stopped and the force was recorded to the nearest 0.1g. Data were expressed as mean ± S.E.M. of the mechanical withdrawal threshold (MWT) in g.

2.5. Thermal hyperalgesia

Thermal hyperalgesia was evaluated by the plantar test (Ugo Basile, Varese, Italy) as described by Guida et al. (2017a). On the day of the experiment, each mouse was placed in a plastic cage (22 x 17 x 14 cm; length x width x height) with a glass floor. After a 30-minute habituation period, the plantar surface of the hind paw was exposed to a beam of radiant heat through the glass floor. The radiant heat source consisted of an infrared bulb (Osram halogen-bellaphot bulb; 8 V, 50 W). A photoelectric cell detected light reflected from the paw and turned off the lamp when the paw movement interrupted the reflected light. The thermal withdrawal latency (TWL) was automatically displayed to the nearest 0.1 s; the cutoff time was set at 20 s to prevent tissue damage. The latency of nociceptive reaction was measured as mean ± S.E.M. of the TWL in seconds.

2.6. Novel object recognition

The experiment was performed as described by D'Agostino et al. (2012) and it started with the habituation period, during which mice were allowed to freely explore for 1 hour the apparatus, which consists of a rectangular open box (40 x 30 x 30 cm; width x length x height) made of gray polyvinyl chloride illuminated by a dim light. The day after, each mouse was allowed to explore 2 identical objects positioned in the back left and right corners for 5 minutes (acquisition). A camera recorded the time spent on exploration of each object. In the test trial, which was conducted 2 hours after the acquisition, 1 of the 2 objects was replaced with a new different object. The time spent exploring the object was the time the mouse spent with its nose directed, and within 1 cm, from the object. The behaviour was recorded and analyzed by a video camera (ANY-MAZE software, Stoelting Co., Wood Dale, IL, USA). Data were expressed as recognition index (R.I.): the percentage of the time the mouse spent exploring the novel object/ the time the mouse spent exploring the novel object + the time the mouse spent exploring the familiar object.

2.7. Morris water maze

Spatial memory was measured by the Morris water maze as described by D'Agostino et al. (2012) that consisted of a round container, 100 cm in diameter and 50 cm in depth. The tank was filled with water (21–26°C) up to a height of 30 cm and the transparent escape platform made of Plexiglas (10 cm in diameter and 29 cm in height) was concealed at 1.5 cm under the surface of water at a fixed place. Swimming was recorded using a camera capture and analyzed using a video tracking software (Any-maze, Stoelting Co., Wood Dale, IL, USA) that divided the pool into four equal quadrants. The platform position remained stable during 5 days in one of the four quadrants. Training phase consisted of four swims per day for 5 days, with about a 15-min inter-trial time. Each of the four starting positions was used in randomized order. Each trial was started by placing a mouse into the pool, facing the wall of the tank and terminated as soon as the animal reach the platform with a cut-off of 60 s. After the test, each mouse was kept warm for an hour and then returned to its home cage. The period spent by the animal to reach the concealed platform was used as the memory index. Average of the four trials for each mouse of each group was expressed as mean ± SEM of the time of latency to reach the platform in seconds for each training day. A probe test was also performed 24 h after the last trial. The platform was removed and each animal was allowed to freely swim for 60 s. The time spent in the quadrant where the platform was previously placed was determined and expressed as mean ± SEM in seconds. A higher percentage of time spent in the platform quadrant is interpreted as a higher level of memory retention.

2.8. Surgical preparation for in vivo field potential recordings at LEC-DG pathway

Briefly, mice C56/BL6J (30-35g, Harlan Laboratories) were first anesthetized with urethane (1.5 g/kg, i.p.) and fixed in a stereotaxic device (David Kopf Instruments, Tujunga, CA, USA). Body temperature was maintained at 37°C with a temperature-controlled heating pad (Harvard Apparatus Limited, Edenbridge, Kent). In all surgical preparations, the scalp was incised and holes were drilled in the skull overlying the site of recording, DG (AP: -2.1 mm from bregma, L: 1.5 mm from midline and V: 1.2 mm below dura) and stimulation, LEC (AP: −4.0 mm from bregma; L:, 4.5 mm from midline and V: 2.9 mm below the dura) according to the coordinates from the atlas of Paxinos and

Franklin (1997) and contralateral with respect to the nerve insult. The stimulating electrode was custom-designed for simultaneously stimulating and administering drugs into the LEC. The stimulating and recording electrodes were lowered slowly in the LEC and DG, respectively, until a field excitatory post-synaptic potential (fEPSP) induced by test pulses (0.2 ms in duration delivered at the frequency of 0.033 Hz) was felt. After a stabilization of the responses, a baseline was recorded for 30 min and a high frequency stimulation (TBS, consisting of 6 trains, 6 bursts, 6 pulses at 400 Hz, interburst interval: 200 ms, intertrain interval: 20 s) was applied in the LEC in order to stimulate the perforant path (PP) fibers for inducing LTP. LTP was considered as an increase in the amplitude and slope of the fEPSPs that exceeded the baseline by 20% and lasted for at least 30 minutes from the TBS. After TBS, the recording of the fEPSPs was continued for 90-120 min. Field recordings were performed with a tungsten microelectrode (1–5 Mohm) and signals were acquired and analyzed with WinLTP software. Electrodes placement was confirmed through evoked responses from stimulation in the LEC as well as histological confirmation. Vehicle or drugs were administered in the LEC by connecting the custom-designed stimulating electrode to a polyethylene tube associated with to a SGE 1μl syringe. Volumes of 600 nl of vehicle or drug solution were injected into the LEC over a period of 60 sec.

2.9. Microdialysis in vivo

Microdialysis experiments were performed in awake and freely moving mice. In brief, mice were anaesthetized with pentobarbital (50 mg/kg, i.p.) and stereotaxically implanted with concentric microdialysis probes into the DG using the coordinates: AP: -1.7 mm, L: 1 mm from bregma and V: 1.8 mm below dura (Paxinos & Franklin, 1997). Dialysis probes, were constructed with 25G (0.3 mm inner diameter, 0.5 mm outer diameter) stainless steel tubing (A-M Systems). Inlet and outlet cannulae (0.04 mm inner diameter, 0.14 mm outer diameter) consisted of fused silica tubing (Scientific Glass Engineering). The probe had a tubular dialysis membrane (Enka AG, Wuppertal, Germany) 1.3 mm in length. Following a recovery period of 24 h, dialysis was commenced with ACSF (NaCl 147 mM, $CaCl_2$ 2.2, KCl 4 mM; pH 7.2) perfused at a rate of 1 μL/min by a Harvard Apparatus infusion pump. Following a 60-min equilibration period, 6 consecutive 30-min dialysate samples were collected. At the end of experiments, mice were anaesthetized and their brains perfused fixed via the left cardiac ventricle with heparinised paraformaldehyde saline (4 %). Brains were dissected out and fixed in a 10 % formaldehyde solution for 2 days. The brain was cut in 40-μm thick slices and observed under a light microscope to identify the probe locations. Dialysates were analyzed through an high performance liquid chromatography method. The system comprised a Varian ternary pump (mod. 9010), a C18 reverse-phase column, a Varian refrigerated autoinjector (mod. 9100), a Varian fluorimetric detector. Dialysates were precolumn derivatized with o-pthaldialdehyde-N-acetylcysteine (OPA-NAC) (10 μl dialysate + 5 μl OPA-NAC + 10 μl borate buffer 10 %) and amino acid conjugates resolved using a gradient separation. The mobile phase consisted of 2 components: 1) 0.2 M sodium phosphates buffer and 0.1 M citric acid (pH 5.8) and 2) 90 % acetonitrile and 10 % distilled water. Gradient composition was determined using an Apple microcomputer installed with Gilson gradient management software. Data were collected using a Dell Corporation PC system 310 interfaced to the detector via a Drew data-collection unit. The mean dialysate concentration of amino acids in the six samples represents the basal release and the results were expressed as the mean ± SEM of the pmol in 10 μl of perfusate (Guida et al., 2015).

2.10. Endocannabinoid levels

The endocannabinoids AEA and 2-AG, and the endocannabinoid-related molecule N palmitoylethanolamide (PEA) were extracted from tissues and then purified and quantified as described previously (Piscitelli et al., 2011). First, tissues were dounce-homogenized and extracted with chloroform/methanol/Tris-HCl 50 mM pH 7.5 (2:1:1, v/v) containing internal deuterated standards for AEA, 2-AG and PEA quantification by isotope dilution (5 pmol of [2H]8AEA, 50 pmol of [2H]52AG, [2H]4 PEA, Cayman Chemicals, MI, USA). The lipid-containing organic phase was dried down, weighed and pre-purified by open bed chromatography on silica gel. Fractions were obtained by eluting the column with 99:1, 90:10 and 50:50 (v/v) chloroform/methanol. The 90:10 fraction was used for AEA, 2-AG and PEA quantification by liquid chromatography-atmospheric pressure chemical ionization-mass spectrometry (LC-APCI-MS), as previously described and using selected ion monitoring at M + 1 values for the four compounds and their deuterated homologues, as described in Piscitelli et al, 2011 (Piscitelli et al., 2011).

2.11. Electron microscopy

Sham and SNI mice treated with vehicle or PEA (n = 3 per group) were deeply anesthetized and perfused transcardially with PBS (pH 7.4) followed by a fixative containing 4% paraformaldehyde and 0.5% glutaraldehyde in 0.1 M phosphate buffer (pH 7.4). Ultrathin sections (60-nm thick) containing the hippocampal DG field were collected serially on Formovar-coated, single- or multiple-slot (50-mesh) grids, stained with 0.65% lead citrate and examined with the Zeiss LEO 912AB transmission electron microscope. In these blinded experiments, synapses were identified based on postsynaptic density, and at least three vesicles in the presynaptic element. Excitatory synapses were identified by their asymmetrical morphology, according to the conventional ultrastructural synaptological analysis described in Cristino et al, 2013 (Cristino et al., 2013). Asymmetrical synapses were counted from n = 25-30 serial ultrathin sections from the DG of brain of each animal covering a total volume of 100-120 μm^3 per brain.

2.12. Immunofluorescence assays

Neurogenesis quantification was performed on 2- months-old C57BL/6J WT, sham and SNI male mice with or without PEA treatment. The animals were deeply anesthetized and transcardially perfused with 4 % paraformaldehyde in 100 mM phosphate buffer, pH 7.4. Coronal sections (10 μm) were cut on a freezing sliding microtome (Leica) and collected on the glass slides in three alternate serial sections. For Ki67 immunohistochemistry, sections were pretreated with phosphate-buffered saline (PBS) and incubated for 1 h at room temperature in PBS containing 0.1 % Triton (PBST) and 5 % appropriate serum (blocking buffer). Sections were then incubated overnight at 4 °C with the following primary antibodies in donkey serum blocking buffer: mouse anti-Ki67 (Abcam 1:200), rabbit anti-NeuN (Abcam; 1:250), goat anti-doublecortin (DCX; Santa Cruz, 1:500), rabbit anti-glial fibrillary acidic protein (GFAP; Abcam 1:200), guinea pig-anti VGluT1 (Synaptic System, 1:1000) rabbit anti-CB1R, mouse anti-β-arrestin2 antibodies revealed by specific Alexa-488 or _546 or _350 secondary donkey anti-IgGs (Invitrogen Life Technology, Paisley, UK) incubated for 2 h at room temperature at 1:200-1:500 dilution range. Sections were counterstained with DAPI (Sigma-Aldrich) to detect nuclei, mounted with Prolong Gold (Invitrogen), and coverslipped. Images were taken with a Nikon confocal microscope through a 20 and 40x objectives.

2.13. Quantification of Ki67-, DCX-positive cells

For the assessment of adult DG neurogenesis, stereological cell counting was performed in serial coronal sections (180 μm pitch) covering the complete rostro-caudal extension of the DG. Fluorescence images were captured with a DMI6000 (Leica, Manheim, Germany) microscope equipped with x-y-z motorized stage, a digital camera Leica DFC 340FX, and the Leica Metamorph imaging software (Leica

MetaMorph AF, Manheim, Germany). Multichannel images were acquired and analyzed using the Leica Application Suite (LAS) AF 2.2.0 software. For each section, z-stack images (2 μm z-step size) covering the complete DG were acquired and DG reconstructed with the MetaMorph software (Leica). Immunopositive cells in the granular cell layer (GCL) and the subgranular zone (SGZ, defined as a 10 μm region below the GCL) were counted by the software. To quantify the CB1R/β-arrestin2 colocalization in the entorhinal cortex z-stack images (2 μm z-step size) covering 100 μm layers II-III were acquired for each section and reconstructed with the MetaMorph software (Leica). Double CB1/β-arrestin2 immunopositive puncta in the 100 μm3 entorhinal cortex were analyzed after thresholding and only yellow CB1R/ β-arrestin2 puncta were counted by the software

2.14. Assessment of DG and hilus volume

For the quantification of DG volumes and hilus, slices were stained with NeuN and acquired by DMI6000 (Leica, Manheim, Germany) microscope equipped with x-y-z motorized stage. The profile area of each section was measured using MetaMorph Imaging Software. The volume estimation of these brain regions was obtained by multiplying the sum of the areas of all sections by the distance between the sections applying the principle of Cavalieri (Gundersen & Jensen, 1987).

2.15. Doublecortin staining and quantification of dendritic arborization

The sections dedicated to the optical doublecortin staining for assessment of dendritic arborization in the DG were incubated with 0.3% triton and 3% normal goat serum (blocking solution) for 2h at room temperature prior to incubation at 4 °C overnight in doublecortin (DCX; Santa Cruz) antibody diluted 1:800 in TBS with 0.3% triton and 1% normal goat serum. Then the sections were washed in TBS and incubate with a biotinylated goat anti mouse (Vector System; 1:400 in TBS) for two hr at room temperature. After washing the sections 3 consecutive times in TBS they were incubated with ABC Lite (1:1.000) for 2 hr at room temperature. Immunostaining was revealed by adding 5 μl of 30% H_2O_2 to one tablet of 10 mg of DAB (3,3″-Diaminobenzidine) solution dissolved in 15 ml of 1 M Tris-HCl (pH 7.6). The sections were washed with ice-cold TBS followed by one wash in TBS at room temperature, dehydratation by using a series of ethanol solutions, cleared in xylene, and then coversliped by using DPX. The quantitative evaluation of dendritic branching was performed on sections immunostained for DCX. Images were acquired with a DMI6000 (Leica, Manheim, Germany) microscope equipped with x-y-z motorized stage and 40x objective by measuring the profile area of each section throught the MetaMoorph Imaging Software. Cell bodies and dendrites were counted from a maximum-intensity projection of a z-series stack by manually tracing lines as described by Rosenzweig and Wojtowicz (Rosenzweig & Wojtowicz, 2011).

2.16. Protein extraction and western blot analysis

For protein extraction, the DG was minced into small pieces with a blender, then suspended in lysis buffer [HEPES 25 mM; EDTA 5 mM; SDS 1%; Triton X-100 1%; PMSF 1 mM; MgCl2 5 mM; Protease Inhibitor Cocktail (Roche, Mannheim, Germany); Phospahatase Inhibitor Cocktail (Roche, Mannheim, Germany)] and cleared by centrifugation (10 min at 10,000 ×g at 4°C). Protein concentration was determined using the method described by Bradford (1976). Each sample was loaded (30 μg), electrophoresed in a 6 or 8 SDS-polyacrylamide gel and electroblotted onto a polyvinylidenedifluoride (PVDF) membrane (EMD Millipore Corp., Billerica, MA, USA). The membrane was blocked in 3% BSA, 1X Tris-buffered saline and 0,01% Tween-20. Primary antibodies to detect GluR1(1:500, Santa Cruz Biotechnology, Santa Cruz, CA, USA), GLU R1 S845(1:500, Abcam, Cambridge, UK), GLUR1 S831 (1:500, MERCK Darmstadt, DE), mGluR1 (1:500, Santa Cruz Biotechnology, Santa Cruz, CA, USA), mGluR7 (1:500, Santa Cruz Biotechnology, Santa Cruz, CA, USA) were used according to the manufacturer's instruction. Immunoreactive signals were detected with a horseradish peroxidase-conjugated secondary antibody and reacted with an ECL system (Amersham Pharmacia, Uppsala, Sweden). Protein levels were normalized with respect to the signal obtained with anti-beta-tubuline monoclonal antibodies (Sigma Chemical Co. 1:1000 dilution). Reactive bands were detected by chemiluminescence (Immobilon western Millipore) on a C-DiGit ® Blot Scanner (LI-COR Biosciences). Images were captured, stored, and analyzed using “Image studio Digits ver. 5.0” software. Bradford M.M. A rapid and sensitive method for the quantization of microgram quantities of protein utilizing the principle of protein-dye binding.

2.17. Statistical analysis

Data were represented as mean ± SEM. Behavioral and electrophysiological data were analyzed by using two-way ANOVA for repeated measures, followed by Bonferroni post hoc test for comparisons between groups and one-way ANOVA, followed by Dunnett's Multiple comparison post hoc test for multiple comparisons within groups. Moreover paired t-test was used for single comparison within groups. Immunohistochemical data were assessed using the D’Agostino-Pearson's normality test. When data were normally distributed, one-way or two-way ANOVA followed by either Dunnett's or Bonferroni's multiple comparison test were used. When the data distribution was not normal, non-parametric Kruskal-Wallis followed by a Dunn's tests were used. P values < 0.05 were considered statistically significant. Statistical analysis was carried out using Prism/Graphpad (GraphPad Software, Inc.) software.

3. Results

3.1. Effect of PEA on mechanical allodynia in sham and SNI wild-type and PPARα null mice

The MWT of sham mice treated with vehicle was 4.36 ± 0.16 g. SNI of the sciatic nerve significantly decreased the MWT of the ipsilateral paw (2.46 ± 0.24 g) in vehicle-treated mice. A 15 days treatment with PEA (10 mg/kg, i.p.) did not change the MWT in sham although it significantly increased it in SNI mice (3.81 ± 0.43 g, $F_{3,24} = 10.70$; $p < 0.0001$), as revealed by one way ANOVA analysis followed by Bonferroni post-hoc test. The MWT of PPAR-α null sham mice was not significantly different from WT sham mice (4.12 ± 0.22 g, $p > 0.05$), as revealed by two-tailed Student's *t*-test. The SNI of the sciatic nerve significantly reduced the MWT in PPAR-α null mice treated with vehicle (2.08 ± 0.33 g). A 15 days treatment with PEA (10 mg/kg, i.p.) did not change the MWT in either sham or SNI PPAR-α null mice (2.60 ± 0.34 g, $F_{3,24} = 8.08$; $p > 0.05$), as revealed by one-way ANOVA analysis followed by Bonferroni post-hoc test (Fig. 1B).

3.2. Effect of PEA on thermal hyperalgesia in sham and SNI wild-type and PPARα null mice

The TWL of sham mice treated with vehicle was 5.72 ± 0.54 s. SNI of the sciatic nerve resulted in a significant decrease in the TWL of the ipsilateral paw (3.52 ± 0.24 s) in vehicle-treated mice. A 15 days treatment with PEA (10 mg/kg, i.p.) did not change the TWL in sham although it significantly increased it in SNI mice (7.8 ± 0.28 s, $F_{3,22} = 15.95$; $p < 0.0001$), as revealed by one way ANOVA analysis followed by Bonferroni post-hoc test. The TWL of sham PPAR-α null mice was not significantly different from WT mice (5.72 ± 0.54 s, $p > 0.05$), as revealed by two-tailed Student's *t*-test. SNI of the sciatic nerve significantly reduced the TWL in PPAR-α null mice (3.67 ± 0.45 s). A 15 days treatment with PEA (10 mg/kg, i.p.) did not change the TWL in either sham or SNI PPAR-α null mice (3.35 ± 0.57 s,

$F_{3,22} = 11.42$; $p > 0.05$), as revealed by one-way ANOVA analysis followed by Bonferroni post-hoc test (Fig. 1C).

3.3. Effect of PEA on discriminative and spatial memory in sham and SNI wild-type and PPARα null mice

In the object recognition test, SNI mice that received vehicle administration showed a significant decrease in the RI (37.33 ± 6.80 %, one way-ANOVA followed by Bonferroni post-hoc test) compared with sham mice that received vehicle administration (64.31 ± 2.88 %) (Fig. 1D). A 15 days treatment with PEA (10 mg/kg, i.p.) did not change the RI in the sham mice whereas it significantly increased it in SNI mice (60.94 ± 5.45 %, $F_{3,21} = 7.84$; $p = 0.0011$). Sham PPARα null mice showed a significant decrease in RI (46.45 ± 4.32 %) compared to the sham WT mice. SNI induced a further, although not significant, reduction of RI in PPARα null mice. A 15 days treatment with PEA (10 mg/kg, i.p.) did not reverse the memory deficit in either sham or SNI PPARα null mice (45.58 ± 4.59 %, $F_{3,14} = 1.14$; $p = 0.36$) (Fig 1D).

In the Morris water maze, SNI mice treated with vehicle showed an increase in the latency to reach the platform at day 2 of the training phase (42.33 ± 5.48 s) compared to sham mice treated with vehicle (26.11 ± 3.37 s), and also at day 3 (31.58 ± 6.99 s *vs* 17.29 ± 2.42 s in sham mice treated with vehicle). The 15 days treatment with PEA (10 mg/kg, i.p.) decreased significantly the latency to reach the platform in SNI mice (26.00 ± 3.5 s) as compared to SNI mice treated with vehicle at day 2 of training (Fig 1F). The 15 days treatment with PEA (10 mg/kg, i.p.) did not change instead the time to reach the platform in the sham. Two-way ANOVA followed by Bonferroni post-hoc test revealed significant differences between treatments ($F_{3,121} = 11.12$, $P < 0.0001$), time ($F_{4,121} = 9.43$, $P < 0.0001$) but no significant difference was found in treatment x time interaction ($F_{12,121} = 0.99$, $P = 0.45$). PPARα null mice did not show any change in the time to reach the platform either after SNI of the sciatic nerve. PEA treatment did not change the latency to reach the platform in either sham or SNI mice. Indeed, two-way ANOVA followed by Bonferroni post-hoc test did not reveal any significant difference between treatments ($F_{3,121} = 9.43$, $P = 0.2$) and no interaction between treatment x time ($F_{12,121} = 0.7$, $P = 0.74$). (Fig. 1G).

SNI mice treated with vehicle showed a significant reduction in the time spent in the target quadrant (16.88 ± 1.48 s) as compared to vehicle-treated sham mice (21.36 ± 2.52 s). A 15 days treatment with PEA (10 mg/kg, i.p.) increased the time spent in the target quadrant in both sham (30.0 ± 1.61 s) and SNI mice (27.0 ± 2.15 s), as assessed by one-way ANOVA followed by Bonferroni post-hoc test ($F_{3,22} = 11.83$, $P < 0.0001$) (Fig. 1H). Sham and SNI PPARα null mice did not show any difference in the time spent in the target quadrant compared to their wild type counterparts (23.84 ± 3.70 s). A 15 days treatment with PEA (10 mg/kg, i.p.) did not change the time spent in the target quadrant in either sham or SNI (19.0 ± 2.74 s, $F_{3,17} = 3.44$; $P = 0.040$) PPARα null mice (Fig. 1H).

3.4. Effect of PEA on LTP at the LEC-DG pathway in sham and SNI wild-type and PPARα null mice

The TBS in the LEC potentiated both amplitude (30–60 min: 211.62 ± 21.6 %; 90-120 min: 266.78 ± 24.3 %, vs 0-30 min: 100%) ($F_{2,42} = 269.5$; $p < 0.0001$) and slope (30– 60 min: 218.42 ± 18.4 %, 90-120 min: 259.66 ± 23.2 %, vs 0-30 min: 100%) ($F_{2,42} = 276.6$; $p < 0.0001$) of the fEPSPs in the DG of sham mice treated with vehicle, one-way ANOVA followed by Dunnet's post hoc test. SNI mice, 30 days post-injury and treated with vehicle, did not show any change of the fEPSP amplitude (30-60 min: 117.4 ± 10.4 %, 90-120 min: 110 ± 13.2 % vs 0-30 min: 99.58 ± 0.55 %) ($F_{2,42} = 31.5$; $p > 0.05$) and slope (30-60 min: 116.1 ± 1.73 %, 90-120 min: 118.5 ± 11.2 % vs 0-30 min: 99.50 ± 0.75%) ($F_{2,42} = 47.6$; $p > 0.05$) after TBS, as assessed by one-way ANOVA followed by Dunnet's post hoc test (Fig. 2E–F, I–J) of fEPSPs. Interestingly, SNI mice treated with vehicle showed input–output curves shifted leftwards compared to vehicle-treated sham mice. Indeed, paired t-test indicated significant changes in the I/O relationship between vehicle-treated sham and SNI mice in the response generated by various stimulus intensities ($t_{0.0100} = 3.686$ $df = 6$ for amplitude, and $t_{0.0036} = 4.627$ $df = 6$ for slope), (Fig. 2B and C).

Chronic treatment with PEA (10 mg/kg, i.p.) did not change LTP in sham mice, except for a slight increase, although not significant, in the slope and amplitude of fEPSPs following the single pulse application. However, this treatment significantly reversed the LTP impairment in SNI mice compared with SNI mice treated with vehicle, 30 days post-injury. Indeed, two-way ANOVA for repeated measures followed by Bonferroni post-hoc test revealed significant differences in the amplitude between treatments ($F_{3,112} = 424.53$, $P < 0.0001$), time ($F_{2,112} = 2280.89$, $P < 0.0001$) and treatment x time interaction ($F_{6,112} = 203.02$, $P < 0.0001$) of EPSPs. Chronic treatment with PEA (10 mg/kg, i.p.) also produced significant differences in the slope between treatments ($F_{3,112} = 565.78$, $P < 0.0001$), time ($F_{2,112} = 2424.50$, $P < 0.0001$) and treatment x time interaction ($F_{6,112} = 216.51$, $P < 0.0001$) of EPSPs. To further explore the involvement of PPARα receptor in the PEA-mediated memory improvement and rescue of LTP in neuropathic conditions, we performed LTP recordings in SNI PPARα null mice, and surprisingly we found a different result respect to the behavioural observations (Fig. 3A, C–F).

Sham and SNI PPARα null mice, 30 days post-injury and treated with vehicle or PEA did not show any difference compared to their WT counterparts in terms of amplitude and slope of fEPSPs after TBS. As for WT mice, two-way ANOVA followed by Bonferroni post-hoc test showed significant differences between treatments ($F_{3,112} = 883.65$, $P < 0.0001$), time ($F_{2,112} = 1552.94$, $P < 0.0001$) and treatment x time interaction ($F_{6,112} = 640.78$, $P < 0.0001$) for the amplitude of EPSPs. Similarly, significant differences were found between treatments ($F_{3,112} = 533.48$, $P < 0.0001$), time ($F_{2,112} = 2516.50$, $P < 0.0001$) and treatment x time interaction ($F_{6,112} = 225.49$, $P < 0.0001$) for the slope of EPSPs (Fig. 3B, G–J).

3.5. Effect of AM251 on LTP at the LEC-DG pathway in sham mice

LEC application of CB1R reverse agonist was performed to explore the specific circuitry LEC-DG pathway in SNI model. The microinjection of AM251 (1 nmol)in the LEC significantly blocked the LTP and induced a decrease in the slope and amplitude of fEPSPs after TBS in the DG of sham mice treated with vehicle. The microinjection of AM251 was performed 15 min before the tetanization and significantly reduced the baseline, simulating a sort of chemical LTD (106.7% at 15 min *vs* 73.23% at 30 min, $t_{0.0001} = 11.09$ $df = 8$ for amplitude and $t_{0.0001} = 13.46$ $df = 8$ for slope). Two-way ANOVA analysis followed by Bonferroni post-hoc test showed significant differences between treatments ($F_{1,56} = 3577.23$, $P < 0.0001$), time ($F_{2,56} = 198.58$, $P < 0.0001$) and treatment x time interaction ($F_{3,56} = 494.3$, $P < 0.0001$) for the amplitude of EPSPs. Similarly, two-way ANOVA analysis followed by Bonferroni post-hoc test showed significant differences between treatments ($F_{1,56} = 2509.53$, $P < 0.0001$), time ($F_{2,56} = 386.89$, $P < 0.0001$) and treatment x time interaction ($F_{3,56} = 793.37$, $P < 0.0001$) for the slope of EPSPs (Fig. 4A–E).

3.6. Effect of PEA on glutamate and GABA release in the DG of sham and SNI mice

The levels of extracellular L-Glu and GABA in the DG of sham and SNI mice treated with vehicle or PEA (10 mg/kg, i.p.) were measured by in vivo microdialysis associated with HPLC (Fig. 4F and G). SNI mice treated with vehicle showed a significant increase in L-Glu (9.57 ± 1.41 pmol/10 μL) compared to sham mice treated with vehicle (4.41 ± 0.65 pmol/10 μL), $F_{3,13} = 9.17$. The chronic treatment with PEA (10 mg/kg, i.p.) decreased extracellular L-Glu in SNI mice (1.51 ± 0.13 pmol/10 μL) although not in sham mice. The levels of extracellular GABA were

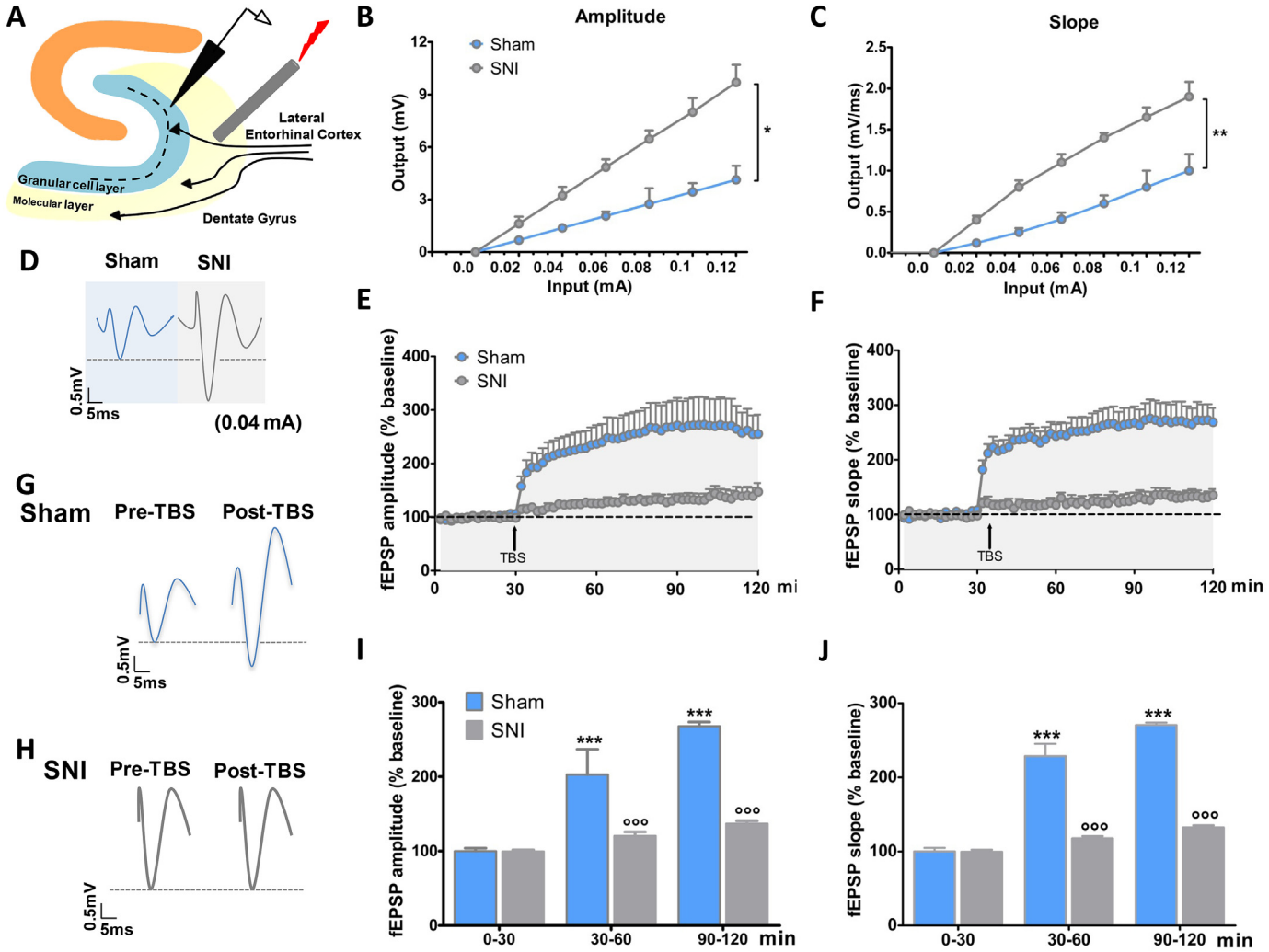

Fig. 2. Long-term potentiation (LTP) in the LEC-DG-pathway in sham and SNI mice. "A" shows a schematic illustration of electrode placements with the stimulating electrode in the LEC for stimulating the lateral perforant path (LPP) fibers and the recording electrode in the DG for recording the fEPSPs of granular cells. "B" and "C" show input-output curves constructed from the fEPSP amplitude and slope vs increasing stimulation intensities at the LEC in sham and SNI mice. "D" shows single EPSPs generated by an electrical stimulation at 0.04 mA in sham and SNI mice. "E" and "F" show time-dependent changes in the fEPSP amplitude and slope after TBS and normalized to baseline in sham and SNI mice. Black arrows represent the TBS application."G" and "H" indicate sample traces of the evoked field potentials recorded in the DG before and after TBS (6 trains, 6 bursts, 6 pulses at 400 Hz, interburst interval: 200 ms) in sham and SNI mice. "I" and "J" show the average of normalized amplitude and slope of fEPSPs at different time points in sham and SNI mice. Data are represented as mean ± SEM of amplitude and slope of fEPSPs. *indicates significant differences *vs* pre-TBS (0-30 min) and °indicates significant differences *vs* sham/veh (n = 10). $P < 0.05$ was considered statistically significant.

not different in sham or SNI mice treated with vehicle or PEA.

3.7. Effect of PEA on endocannabinoids levels in the LEC of sham and SNI mice

Levels of 2-AG significantly increased after the chronic treatment with PEA (10 mg/kg, i.p.) in both the ipsi and contra-lateral side to nerve lesion of the LEC in sham mice compared to sham mice treated with vehicle ($P < 0.001$). No significant differences were observed in *N*-acylethanolamine levels (AEA and PEA, Fig. 4) between vehicle or PEA-treated sham and SNI mice. 2-AG levels increased in both the ipsi and contra-lateral side of the LEC in SNI mice treated with vehicle compared to the vehicle-treated sham mice ($P < 0.001$). PEA treatment seemed to reverse this effect in the SNI mice, even though not significantly.

3.8. Effect of PEA on glutamate receptor expression in the DG of sham and SNI mice

Western blotting was carried on the DG obtained from sham or SNI mice treated with vehicle or PEA (10 mg/kg, i.p.). SNI of the sciatic nerve induced a significant increase in mGluR1 (0.21 ± 0.04; $F_{3,8} = 14.05$; $p < 0.01$) (Fig. 5F) and mGluR7 (0.28 ± 0.02; $F_{3,8} = 15.82$; $p < 0.05$) (Fig. 5G) as compared with sham mice treated with vehicle respectively (0.02 ± 0.005 and 0.04 ± 0.02, respectively). Furthermore, SNI induced a significant increase in the GluR1 (4.46 ± 0.45; F3,8 = 11.84; $p < 0.01$), GluR1-s845 (0.0003 ± 4.493e-005; $F_{3,8} = 10.51$; $p < 0.01$) and GluR1-s831 (0.0003 ± 6.854e-005; $F_{3,8} = 14.64$; $p < 0.01$) subunits of AMPA receptor (Fig. 5C, D and E) of SNI mice compared with sham mice treated with vehicle (1.05 ± 0.17; 6.129e-005 ± 4.132e-005 and 2.696e-005 ± 1.803e-005, respectively). No changes in the mGluR1 (0.19 ± 0.02) and mGluR7 (0.38 ± 0.09) protein levels were observed in SNI mice treated with PEA (10 mg/kg, i.p.) compared to SNI mice treated with vehicle. Moreover, after the chronic treatment with PEA (10 mg/kg, i.p.) SNI mice showed a

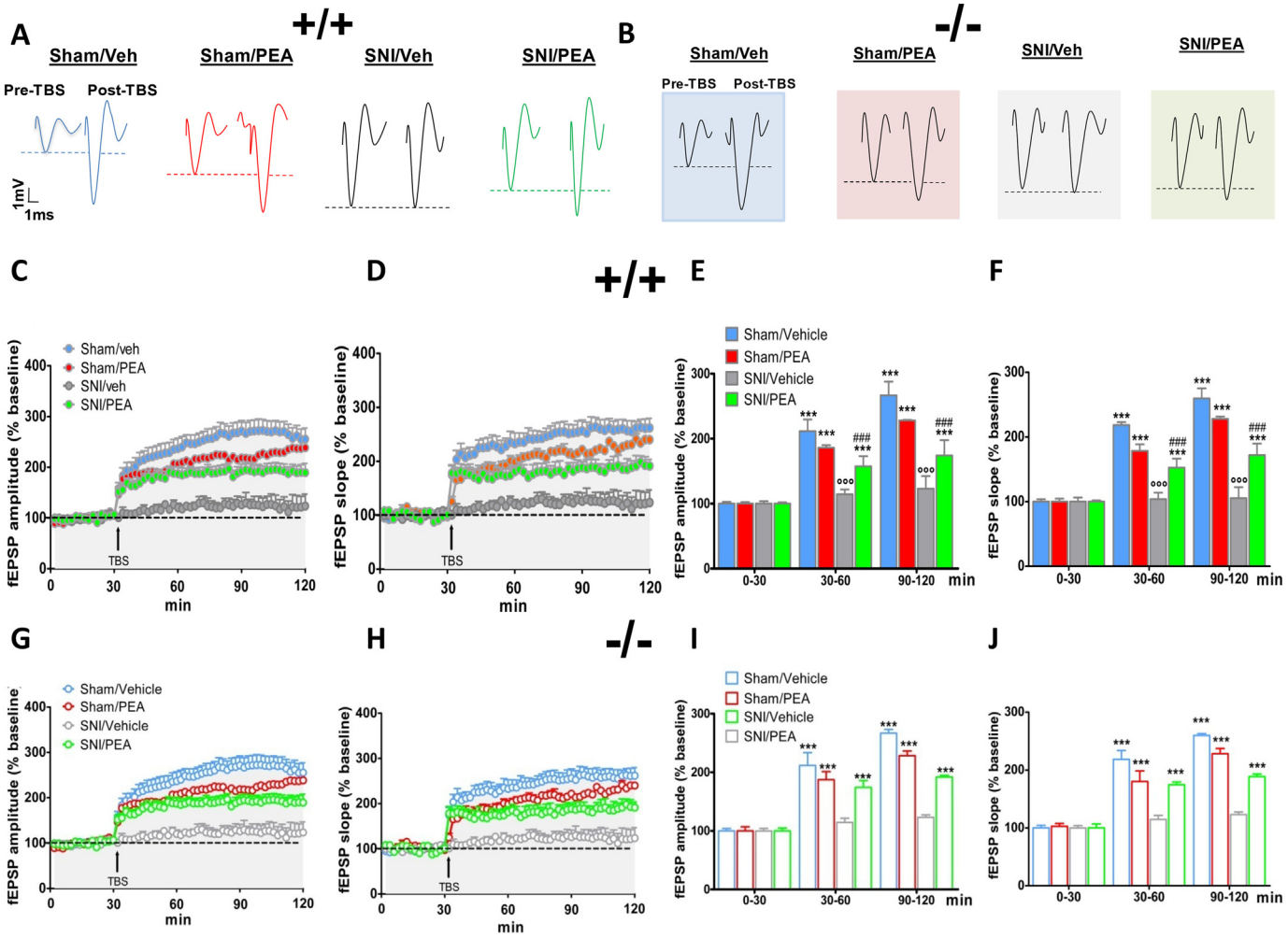

Fig. 3. Effect of vehicle or PEA on long term potentiation at the LEC-DG pathway in sham and SNI WT and PPARα null mice. "A and B" show sample traces of a single evoked fEPSP recorded in the DG before and after TBS in sham and SNI WT or PPARα null mice treated with vehicle or PEA. "C" and "D" show time-dependent changes in the fEPSP amplitude and slope after TBS normalized to baseline in sham and SNI WT mice treated with vehicle or PEA. "E" and "F" show the average of normalized amplitude and slope of fEPSPs before and after TBS at different time points in sham and SNI WT mice treated with vehicle or PEA. "G" and "H" show time-dependent changes in the fEPSP amplitude and slope after TBS normalized to baseline in sham and SNI PPARα null mice treated with vehicle or PEA. "I" and "J" show the average of normalized amplitude and slope of fEPSPs before and after TBS at different time points in sham and SNI PPARα null mice treated with vehicle or PEA. The black arrows represent the TBS application. Data are represented as mean ± SEM of fEPSPs amplitude and slope. *indicate significant differences *vs* pre-TBS (0-30 min), °indicate significant differences *vs* sham/veh and #indicate significant differences *vs* SNI/veh (n = 10). $P < 0.05$ was considered statistically significant.

significant decrease in GluR1 (1.56 ± 0.72; $p < 0.05$), GluR1-s845 (2.833e-005 ± 1.783e-005; $p < 0.01$) and GluR1-s831 (4.986e-005 ± 1.501e-005; $p < 0.01$) protein levels compared to SNI mice treated with vehicle.

3.9. Effect of PEA on postsynaptic density and adult neurogenesis in the DG of sham and SNI mice

In the light of the dramatic impairment of postsynaptic plasticity observed in the LEC-DG pathway of SNI mice, we investigated the effect of SNI on the synaptic arrangement of excitatory inputs to hippocampal DG by performing unbiased electron microscopy according to Cristino, et al, (2013) [32]by applying the morphological method that identifies excitatory synapses by their asymmetrical morphology. Analysis of variance (ANOVA) across different groups revealed a robust loss of asymmetrical synapses, i.e. putative excitatory synapses, at both axosomatic and axodendritic compartments of the hilus in SNI mice as compared to sham mice (SNI = 22.3 ± 1.8 *vs* sham = 38.6 ± 3.4; $p < 0.01$) (Fig. 5A and B). Interestingly, PEA injection reversed this condition in SNI mice whereas was ineffective in sham mice (SNI/PEA = 34.7 ± 4.5 *vs* sham = 36.5 ± 4.6) (Fig. 5A and B). To further determine the effect of SNI on the synaptic arrangement of excitatory inputs to DG and neurogenesis we next investigated the neuroanatomical features of the DG in sham and SNI mice. To this aim, we used Ki67/DCX/GFAP immunohistochemistry. The number of Ki67(+)-positive cells was significantly decreased in SNI mice, indicating a marked reduction in hippocampal progenitor proliferation (Fig. 5C). Similarly, the quantification of the total number of cells positive for DCX, a marker of neuroblasts and newly generated neurons, revealed a significant decrease in SNI mice, suggesting that the impairment in proliferation produces a parallel decrease in the number of newborn neurons (Fig. 5C). This effect was reversed by PEA treatment (Fig. 5D) as compared to their respective sham and SNI vehicle-treated mice. Differentiation of the surviving progenitors into glia or neurons was also examined respectively by Ki67 co-labeling with the astrocyte marker GFAP (Fig. 5C) and DCX positive cells with the mature neuronal marker NeuN (Fig. 5D). Since numerous reports suggest that spinal nerve injury may alter the length and branching complexity of dendritic arbors in the DG (Parekh & Ascoli, 2016) we therefore examined the dendritic development of DG newborn DCX-positive granule cells in the different

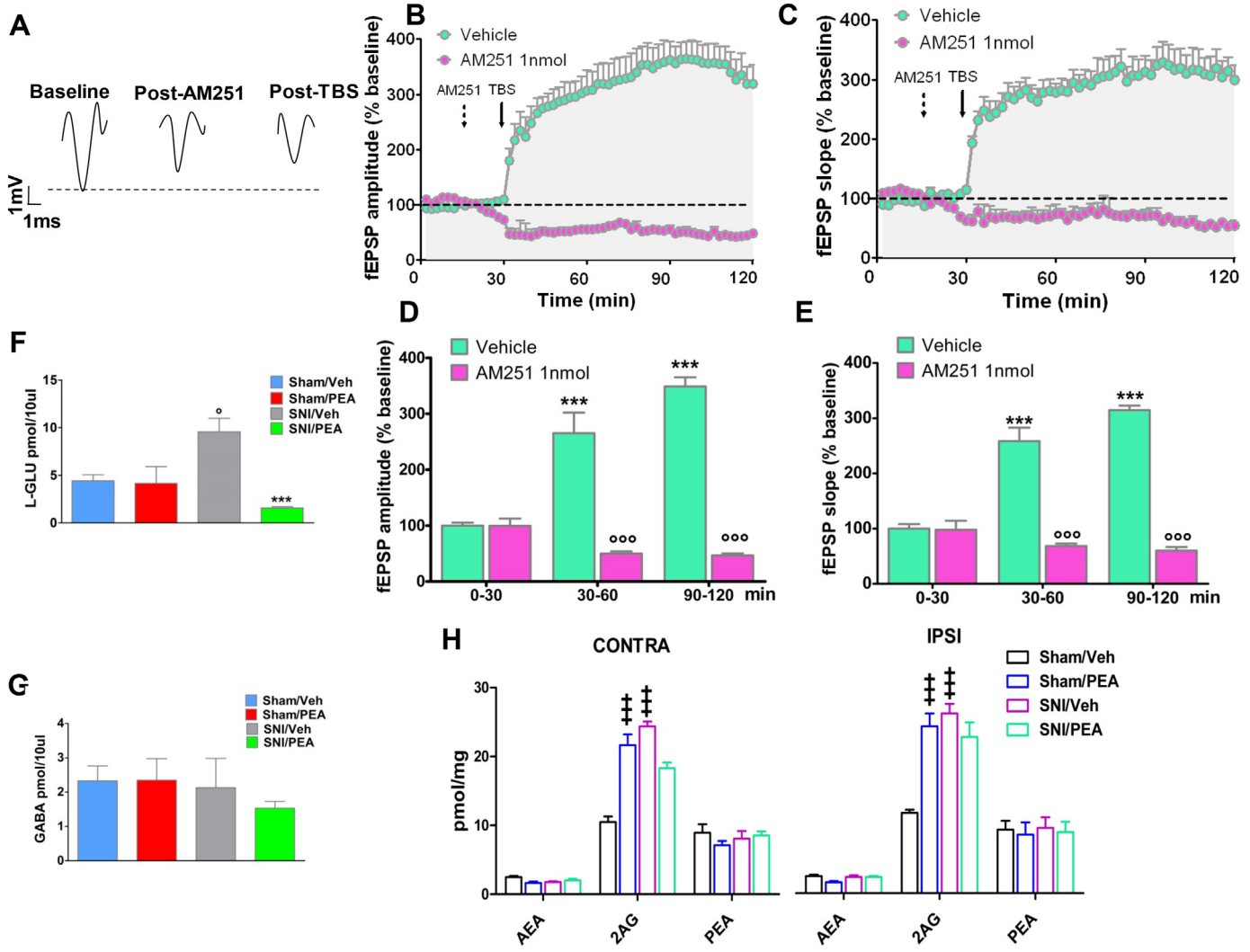

Fig. 4. "A" shows the effect of a single microinjection of AM251 (1 nmol) on the sample trace of a single evoked fEPSP recorded in the DG before and after TBS in sham mice. "B" and "C" show the effect of a single microinjection of AM251 in the LEC on the time-dependent amplitude and slope of fEPSPs in the DG after TBS and normalized to baseline in sham WT mice. "D" and "E" show the effect of a single microinjection of AM251 on the average of normalized amplitude and slope of fEPSPs before and after TBS at different time points in sham WT mice. "F" and "G" show the effect of vehicle or PEA on the extracellular level of L-Glu and GABA in the DG of sham and SNI mice "H" shows the effect of vehicle or PEA on the levels of the endocannabinoid anadamide (AEA), 2-arachydonoylglycerol (2-AG) and PEA in the LEC in sham and SNI mice. Data are represented as mean ± SEM of fEPSPs amplitude and slope (D and E). °indicates significant differences vs vehicle (D and E) or sham/veh (F and H), *indicates significant differences vs SNI/veh (n= 10). $P < 0.05$ was considered statistically significant.

groups of mice. Branch order analysis showed that primary basal dendrites were not affected by SNI, whereas higher-order dendrites were significantly reduced compared to sham (either vehicle or PEA treated). PEA was able to rescue the integrity of higher-order dendrites in SNI mice as well as the volume of the DG, which was reduced compared to sham mice (Fig. 5D). As shown in previous studies for other brain regions (Breivogel et al., 2013; Imperatore et al., 2016), we found here also in the LPP a significant CB1 co-distribution with β-arrestin2, suggesting that β-arrestin2 might regulate CB1 signaling in this area. Indeed, CB1 and β-arrestin2 co-distribution was higher in the LPP of SNI mice as compared to sham mice, suggesting the presence of a strongly increased CB1 internalization in neuropathic mice, which underlies a β-arrestin2-mediated CB1 desensitization in SNI mice with abnormally elevated 2-AG levels (Fig. 6E). Double CB1/β-arrestin2 markers strongly co-localized in the LEC of SNI mice showing a percentage of immunopositive puncta over 23.6 ± 2.7% volume in 100 μm3 LEC in comparison to sham (12.8 ± 1.2% and 15.4 ± 1.8% volume /100 μm3 LEC, respectively for vehicle- and PEA-treated mice; $P < 0.005$; n = 3 mice per group), and to PEA-treated SNI mice (10.7 ± 0.9% volume in 100 μm^3 LEC; $P < 0.005$; n = 3 mice per group).

4. Discussion

The SNI induced thermal hyperalgesia, mechanical allodynia and cognitive deficits consistently with affective/cognitive impairments associated with neuropathic pain in both, humans and rodents (Moriarty et al., 2011; Walker et al., 2013; Yalcin et al., 2011). SNI impaired also the LTP at the LEC-DG pathway, compromising the flow of inputs likely associated with the cognitive impairment (Bailey & Kandel, 1993; Bekinschtein et al., 2008). This loss in LTP induction was associated with a higher basal amplitude and slope in response to the single pulse, possibly due to the increase of glutamate in SNI mice. Chronic pain-related cognitive deficits in both humans and rodents are long-lasting and this cannot be only explained by synaptic functional changes (Holtmaat & Svoboda, 2009). The loss of LTP at the LEC-DG pathway was associated here with a reduction of postsynaptic density, apical dendrites and mossy fibers length, Ki67-positive proliferating cells and DCX-positive neurogenic precursors in the DG of SNI mice. SNI

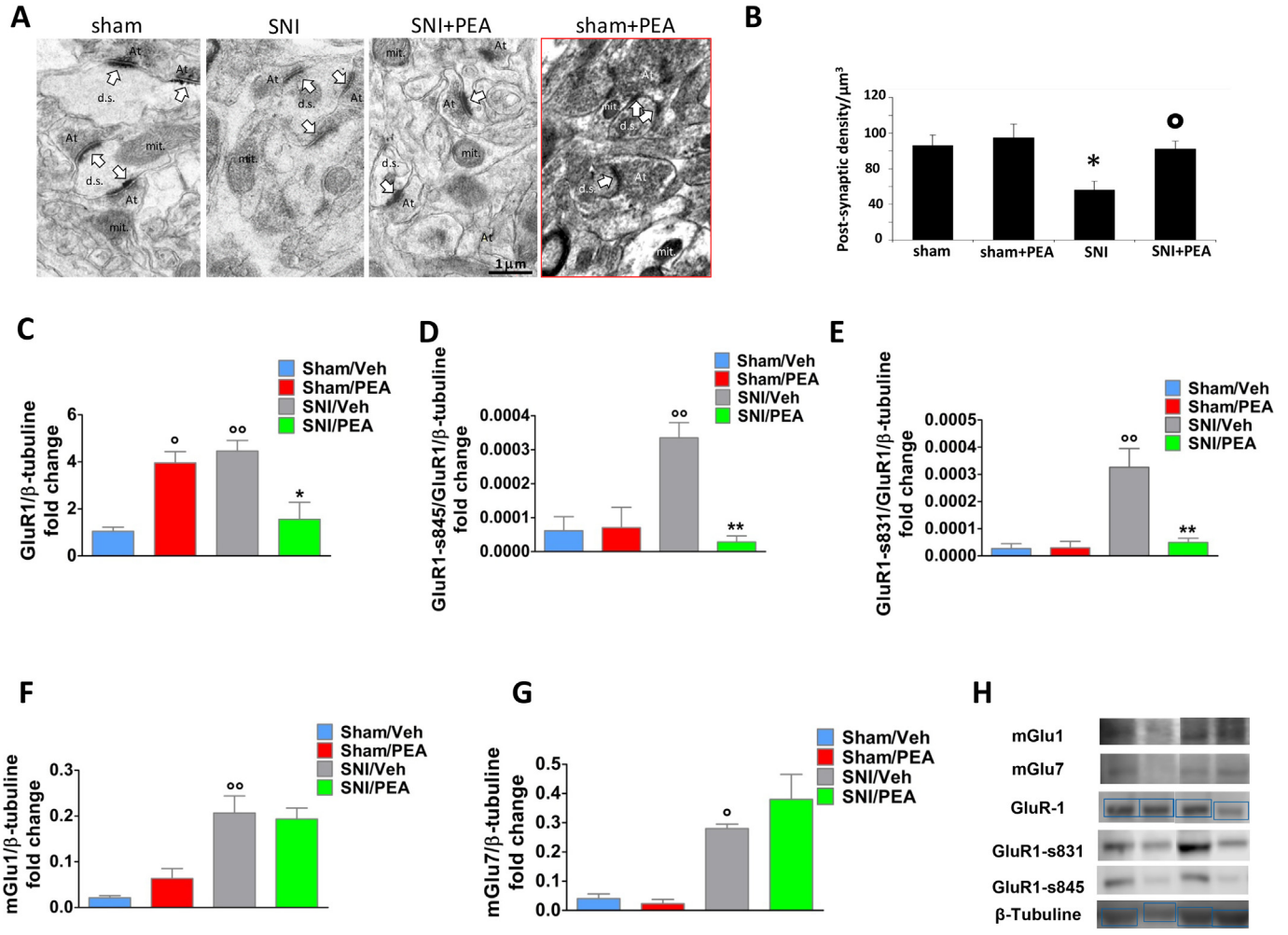

Fig. 5. "A" shows low density of asymmetrical synapses i.e. putative excitatory synapses, at somatodendritic compartment of DG (arrows) of SNI wild-type mice. Dendritic spine (d.s.); mithocondria (mit); axon terminal (At). (Scale bar, 0.3 µm). "B" shows Bar graph showing the mean number of asymmetrical synapses per ≅ 100 µm^3 of DG (n = 3) covering ≅ 24 consecutive serial ultrathin sections per mouse. "C", "D", "E, "F" and "G" show the quantification of the protein expression levels of GluR1, GluR1-s845, GluR1-s831, mGlu1 and mGlu7 in the DG of sham and SNI mice treated with vehicle or PEA, respectively. H" shows the western blots of GluR1, GluR1-s845, GluR1-s831, mGlu1 and mGlu7 proteins (n = 4-5). Data are expressed as mean ± SEM of the arbitrary units, quantified with respect to housekeeping β-tubuline protein.

mice also showed alterations in the expression of GluR1 and GluR1s845 and GluR1s831 subunits of AMPA receptors. An increase in mTOR-induced phospho-Akt and phospho-S6 activity has been already found in SNI mice with cognitive and affective decline (Lyu et al., 2013). The enhanced insertion of AMPA receptors represents a maladaptive phenomenon in neuropathic pain or neurological/psychiatric diseases (Sestito et al., 2010; Chen et al., 2014a). SNI mice showed an increased mGluR1 and mGluR7 expression. The mGluR7 increase, which for its low affinity is recruited under high glutamate concentration (Palazzo et al., 2015), may counteract excessive NMDA stimulation and excitotoxicity in SNI conditions. Changes in mGluR expression were found in chronic pain models (Palazzo et al., 2013; Rossi et al., 2014; Koga et al., 2016; Schoepp et al., n.d.). The increased mGluR1 expression could be a maladaptive response, since it enhances NMDA activity, however NMDA receptor leads to BDNF release/mTOR signaling and consequent neurogenesis (Ryskalin et al., 2017). The SNI increased glutamate level in the DG proposed as crucial mechanism underlying neuropathic pain (Chung et al., 2017). The GABA levels were instead unmodified possibly for counteracting glutamatergic hyperactivity. Moreover, we observed an increase in 2-AG whereas AEA and PEA levels, remained unmodified in the LEC of SNI mice. The increase in 2-AG biosynthesis may be caused by glutamate mGluR5 stimulation in dendrite spines (Katona et al., 2006; Jung et al., 2012). 2-AG would in turn reduce further release (Wang, 2003), LEC over-activity during glutamate excitotoxicity (Maejima et al., 2005; Marcaggi & Attwell, 2005; Rancz & Häusser, 2006; Lo Verme et al., 2005). Alternatively, elevation of 2-AG level might cause CB1 receptor desensitization, observed in the LEC as increased CB1 co-localization with β-arrestin and internalization. In this case, up-regulation of 2-AG could be a maladaptive response to SNI, underlying impaired LTP in the DG, a type of synaptic plasticity, found here to be mediated by CB1 receptors. Indeed, 2-AG activates CB1 and CB2 with analgesic/neuroprotective actions (Lo Verme et al., 2005), thereby modulating, pain transmission (Palazzo et al., 2010), whereas AEA can only activate CB1, but can instead gate TRPV1 channels, and PEA was shown to act on GPR55, TRPV1 and PPAR-α (Ambrosino et al., 2013).

The analgesic effect of PEA (Lo Verme et al., 2005; Petrosino et al., 2010) was obtained here even by starting the treatment two weeks after the SNI surgery, comparable to an advanced stage of neuropathy in humans (Truini et al., 2013). PEA also improved object recognition and Morris water maze tasks and this (Guida et al., 2015; Guida et al., 2017a) correlates with the rescue of LTP in the LEC-DG pathway in SNI mice and PEA-induced increase in 2-AG level in the LEC of SNI mice. Indeed, a 2-AG-dependent synaptic potentiation at lateral perforant path (LPP)-DG pathway has been described (Wang et al., 2016): it initiates through mGluR5 and NMDA stimulation, Ca2 + -mediated DAGL-

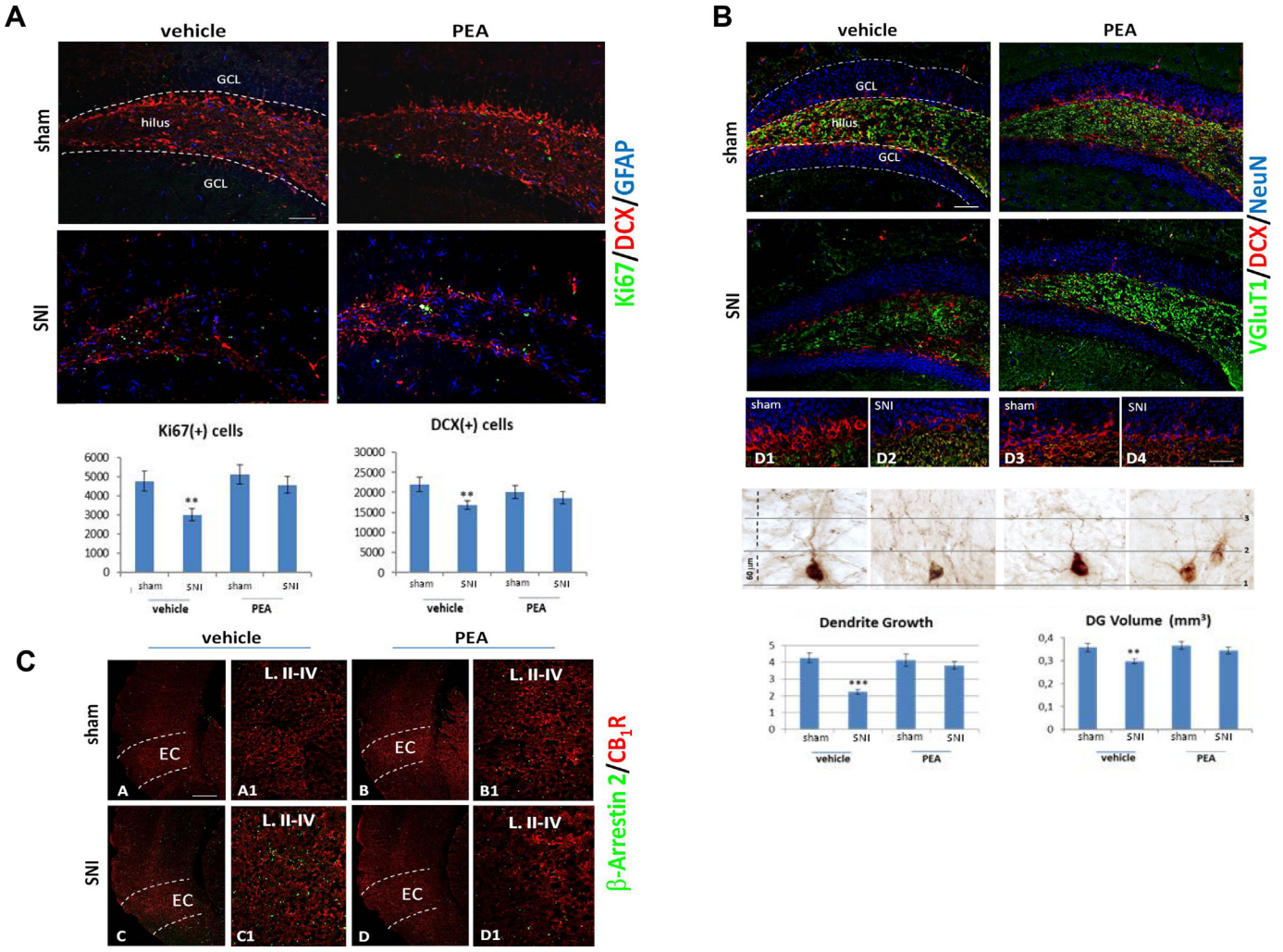

Fig. 6. "A" shows hippocampal neuronal progenitors proliferation (Ki67, green) and neuronal survival (DCX, red) and glial (GFAP, blue) differentiation from representative images of DG sections of wild-type mice. Scale bar: 100 μm. Quantification of Ki67 and DCX immunoreactive cells in the subgranular zone of DG of sham and SNI mice I represented in the bar graphs (n = 3). "B" shows hippocampal neuronal progenitors differentiation (DCX, red), excitatory glutammatergic input (VGluT1, green) and neuronal survival (NeuN, blue) labeling from representative images of DG sections from mice. Scale bar: 100 μm. Analysis of dendrites growth in DCX-positive cells (red) from sham/vehicle (A1), SNI/vehicle (B1), sham/PEA (C1) and SNI/PEA (D1) mice were revealed by optical immunohistochemical images of DCX-labeled neurons from DG sections. Bar graphs show the number primary dendrites and DG volume (B left and right, respectively). "C" shows representative confocal images of CB1R/β-arrestin2 immunohistochemical labeling of lateral entorhinal cortex EC, layers II-IV (A-D). (A1-D1) Higher magnification of the respective fields outlined in A-D. Scale bar: 200μm (A-D) and 100μm (A1-D1). Scale bar is x μm. Data are presented as mean ± S.E.M. $^{**}p < 0.01$, $^{***}p < 0.001$ vs sham/vehicle.

α activation and 2-AG production, which serving as retrograde messanger enhances glutamate release, via CB1 stimulation (Palazzo et al., 2012). Pertinent to this, AM251, a CB1 inverse agonist, reduced the amplitude and slope of fEPSPs (suggesting a tonic role of the CB1 for maintaining synaptic plasticity) and prevented the LTP induction in the LEC-DG pathway. However, PEA increased 2-AG levels in sham mice, but tended to decrease them in SNI mice, suggesting that the reversal of LTP impairment by PEA was due to other effects (see below). On the other hand, the stimulation of 2-AG levels, which has been reported also in the dog skin, in human keratinocytes and plasma (Petrosino et al., 2016), as well as in the mouse striatum (Musella et al., 2017), could facilitate synaptic potentiation in the DG under physiological conditions (i.e. without SNI-induced CB1 internalization/desensitization). Accordingly, we found that PEA enhanced the fEPSP and produced a rapid learning in sham mice. PEA could thus produce a nootropic effect in physiological conditions supporting the tight correlation between PPARα signaling, entorhinal cortex-dentate gyrus pathway and cognition. Intriguingly, we found a significant increase in 2-AG levels also in untreated SNI mice, where impairments in memory and LTP were found. A CB1 receptor desensitization in neuropathic pain (Parekh & Ascoli, 2016; Palazzo et al., 2012) via G protein-coupled receptor kinase and β-arrestin2 binding, has been described (Violin et al., 2006; Smith & Rajagopal, 2016). Consistently, we found in the LPP of SNI mice a significant CB1 receptor co-distribution with β-arrestin2, whose expression was higher in the SNI mice, suggesting a strong CB1 internalization, reversed by PEA, which also restored LTP.

The treatment with PEA normalized synaptogenesis, which is at the base of the cognitive ability (Saxe et al., 2006). It indeed restored the loss of postsynaptic density and increased the number of neuroblasts and newly generated neurons in SNI mice, whereas it was devoid of activity in sham mice. PEA was able to rescue the integrity of higher-order dendrites as well as the volumes of the DG, which were reduced in SNI mice. The effect of PEA at increasing synaptogenesis correlated with the improvement of episodic memory and LTP in SNI mice. PEA treatment in SNI mice has proved to increase the levels BDNF promoting neurogenesis (Bekinschtein et al., 2008). PEA treatment also decreased the GluR1, GluR1s845 and GluR1s831 subunits of AMPA receptors, the increase of which is associated with behavioral symptoms

following peripheral injury (Chen et al., 2014b). We observed a trend of PEA to increase GluR1 expression (although not significant) in sham mice, consistently with the facilitation of AMPA-mediated EPSPs in pyramidal neurons of the DG in sham mice treated with PEA. PEA also tended to increase mGluR7 expression (although not significantly) in SNI mice. The increase in mGluR7 expression has been found to be associated with the rescue of cognitive and social (Gogliotti et al., 2017), though not affective (Wieronska & Pilc, 2009) behavior. Finally, PEA also tended to elevate reactive astrogliosis in the DG, which, based on the anti-inflammatory nature of this compound and on its beneficial actions observed in this study, could be interpreted with such phenomenon playing a role in the resolution of neuroinflammation rather than in its exacerbation, possibly via indirect activation of CB2 receptor (Ortega-Gutiérrez et al., 2005), as previously demonstrated in microglia (Guida et al., 2015).

PEA treatment also counteracted the glutamate increase likely associated with the recovery of LTP induction in the SNI mice, in which the basal amplitude and slope of single pulses were already high, preventing a further potentiation after tetanus application in the LEC. The treatment with PEA did not change the levels of GABA, PEA and AEA in sham or SNI mice, whereas, as discussed above, it increased the levels of 2-AG in sham mice. The lack of effect of PEA in changing the level of AEA and PEA was not completely unexpected and found in other or the same experimental models (Guida et al., 2017a; Petrosino et al., 2016). The PEA effect in increasing the 2-AG levels in healthy conditions was recently reported and associated to the PEA “entourage effect (Guida et al., 2015; Petrosino et al., 2016). The effect of PEA at increasing 2-AG level is unlikely associated with an inhibition of 2-AG metabolizing enzymes since: i) the time of the increase in 2-AG level is not compatible with transcriptional modulation (Petrosino et al., 2016), ii) monoacyglycerol lipase, the main enzyme degrading 2-AG (Blankman et al., 2007), is not inhibited by PEA, and iii) the inhibition of other hydrolases degrading 2-AG under certain circumstances, including FAAH (Goparaju et al., 1998), is denied by the lack of effect of PEA on AEA and PEA levels. The effect of PEA through other targets such as PPARα, GPR55 or GPR119 (Ryberg et al., 2007; Godlewski et al., 2009) is also unlikely since 2-AG increase is associated with Gq/11-coupled receptors and none of these receptors is associated with Gq/11. Due to the promiscuity of sites of action of PEA, the possibility that an unknown target associated with PLC and 2-AG synthesis cannot be excluded and deserves other investigations. The antinflammatory (Lo Verme et al., 2005), analgesic (Suardíaz et al., 2007) and neuroprotective (Di Cesare Mannelli et al., 2015) effects of PEA are associated with PPARα stimulation. In order to identify PPARα mediated effects induced by PEA we carried out part of the experiments in PPARα knock-out mice. PEA reversed thermal hyperalgesia, mechanical allodynia and cognitive impairments in SNI wild type, though not PPARα null, mice as already reported (D'Agostino et al., 2015). Intriguingly, PEA chronic treatment partially rescued the compromised LTP in LPP-DG pathway also in PPARα null mice. This functional compensation to PPARα deletion, which limits knock-out mice strategies may underlie the dissociation between PEA action on sensory/cognitive behavior, functional processes involving several highly integrated pathways and brain areas and LTP, an activity within a single neural circuitry. If a possible mechanism for PEA effect on LTP involves its reversal of CB1 receptor desensitization likely it does not require PPARα

but instead other targets, such as TRPV1, whose activation (Marsch et al., 2007; Zschenderlein et al., 2011; Hurtado-Zavala et al., 2017) or desensitization (Banke, 2016), mediate LTP in hippocampus and entorhinal cortex. In conclusion, PEA ameliorates pain, cognitive behavior, and normalizes LTP and neuroanatomical deleterious alterations in the DG of SNI mice, these effects being mostly absent in PPARα deficient mice. PEA promotes the hippocampal synaptic plasticity and behavioral cognitive flexibility also in physiological conditions, indicating a nootropic effect.

Acknowledgements

We would like to thank Dr. Yu Tian Wang and his research group from University of British Columbia (UBC), Vancouver, Canada, for technical support on electrophysiology LTP *in vivo* recordings. The study is supported by the FIRB 2012 of Livio Luongo code RBFR126IGO.

Conflict of interest

None of the other authors have any conflicts of interest to declare.

Appendix A. Supplementary data

Supplementary data to this article can be found online at https://doi.org/10.1016/j.nbd.2018.09.023.

References

Ambrosino, P., Soldovieri, M.V., Russo, C., Taglialatela, M., et al., 2013. Bailey CH, Kandel ER (1993) Structural changes accompanying memory storage. Annu Rev Physiol 55, 397–426.
Bailey, C.H., Kandel, E.R., 1993. Structural changes accompanying memory storage. Annu Rev Physiol 55, 397–426 Review.
Banke, T.G., 2016. Inhibition of TRPV1 channels enables long-term potentiation in the entorhinal cortex. Pflugers Arch 468 (4), 717–726.
Bekinschtein, P., Cammarota, M., Katche, C., Slipczuk, L., Rossato, J.I., Goldin, A., et al., 2008. BDNF is essential to promote persistence of long-term memory storage. Proc Natl Acad Sci U SA 105 (7), 2711–2716.
Blankman, J.L., Simon, G.M., Cravatt, B.F., 2007. A comprehensive profile of brain enzymes that hydrolyze the endocannabinoid 2-arachidonoylglycerol. Chem Biol (12), 1347–1356.
Breivogel, C.S., Puri, V., Lambert, J.M., Hill, D.K., Huffman, J.W., Razdan, R.K., et al., 2013. The influence of beta-arrestin2 on cannabinoid CB1 receptor coupling to G-proteins and subcellular localization and relative levels of beta-arrestin1 and 2 in mouse brain. J Recept Signal Transduct Res 33 (6), 367–379.
Bush, D., Caswell, B., Burgess, N., 2014. What do grid cells contribute to place cell firing? Trends Neurosci 37 (3), 136–145.
Chen, T., Wang, W., Dong, Y.L., Zhang, M.M., Wang, J., Koga, K., et al., 2014a. Postsynaptic insertion of AMPA receptor onto cortical pyramidal neurons in the anterior cingulate cortex after peripheral nerve injury. Mol Brain 7, 76.
Chen, X., Liao, Z., Wong, Y.T., Guo, Y., He, J., 2014b. Time course of the dependence of associative memory retrieval on the entorhinal cortex. Neurobiol Learn Mem 116, 155–161.
Chung, G., Kim, C.Y., Yun, Y.C., Yoon, S.H., Kim, M.H., Kim, Y.K., et al., 2017. Upregulation of prefrontal metabotropic glutamate receptor 5 mediates neuropathic pain and negative mood symptoms after spinal nerve injury in rats. Sci Rep 7, 9743.
Cristino, L., Busetto, G., Imperatore, R., Ferrandino, I., Palomba, L., Silvestri, C., et al., 2013. Obesity-driven synaptic remodeling affects endocannabinoid control of orexinergic neurons. Proc Natl Acad Sci U S A 110 (24), E2229–E2238.
D'Agostino, G., Russo, R., Avagliano, C., Cristiano, C., Meli, R., Calignano, A., Jun 2012. Palmitoylethanolamide protects against the amyloid-β25-35-induced learning and memory impairment in mice, an experimental model of Alzheimer disease. Neuropsychopharmacology. 37 (7), 1784–1792.
D'Agostino, G., Cristiano, C., Lyons, D.J., Citraro, R., Russo, E., Avagliano, C., et al., 2015. Peroxisome proliferator-activated receptor alpha plays a crucial role in behavioral repetition and cognitive flexibility in mice. Mol Metab 4 (7), 528–536.
Decosterd, I., Woolf, C.J., 2000. Spared nerve injury: an animal model of persistent peripheral neuropathic pain. Pain 87 (2), 149–158.
Dellarole, A., Morton, P., Brambilla, R., Walters, W., Summers, S., Bernardes, D., et al., 2014. Neuropathic pain-induced depressive-like behavior and hippocampal neurogenesis and plasticity are dependent on TNFR1 signaling. Brain Behav Immun 41, 65–81.
Di Cesare Mannelli, L., Pacini, A., Corti, F., Boccella, S., Luongo, L., Esposito, E., et al., 2015. Antineuropathic profile of N-palmitoylethanolamine in a rat model of oxaliplatin-induced neurotoxicity. PLoS One 10 (6), e0128080.
Fusco, R., Gugliandolo, E., Campolo, M., Evangelista, M., Di Paola, R., Cuzzocrea, S., Jul 25, 2018. Effect of a new formulation of micronized and ultramicronized N-palmitoylethanolamine in a tibia fracture mouse model of complex regional pain syndrome. PLoS One 13 (7), e0201501.
Giordano, C., Cristino, L., Luongo, L., Siniscalco, D., Petrosino, S., Piscitelli, F., et al., 2012. TRPV1-dependent and -independent alterations in the limbic cortex of neuropathic mice: impact on glial caspases and pain perception. Cereb Cortex 22 (11), 2495–2518.
Godlewski, G., Offertáler, L., Wagner, J.A., Kunos, G., 2009. Receptors for acylethanolamides-GPR55 and GPR119. Prostaglandins Other Lipid Mediat 89 (3-4), 105–111.
Gogliotti, R.G., Senter, R.K., Fisher, N.M., Adams, J., Zamorano, R., Walker, A.G., et al., 2017. mGlu(7) potentiation rescues cognitive, social, and respiratory phenotypes in a mouse model of Rett syndrome. Sci Transl Med 9 (403).
Gol, A., Faibish, G.M., 1966. Hippocampectomy for relief of intractable pain. Tex Med 62,

76–79.
Goparaju, S.K., Ueda, N., Yamaguchi, H., Yamamoto, S., 1998. Anandamide amidohydrolase reacting with 2-arachidonoylglycerol, another cannabinoid receptor ligand. FEBS Lett 23 (422(1)), 69–73.
Grilli, M., 2017. Chronic pain and adult hippocampal neurogenesis: translational implications from preclinical studies. J Pain Res 10, 2281–2286.
Guida, F., Luongo, L., Marmo, F., Roma, R., Iannotta, M., Napolitano, F., et al., 2015. Palmitoylethanolamide reduces pain-related behaviors and restores glutamatergic synapses homeostasis in the medial prefrontal cortex of neuropathic mice. Mol Brain 8, 47.
Guida, F., Boccella, S., Iannotta, M., De Gregorio, D., Giordano, C., Belardo, C., et al., 2017a. Palmitoylethanolamide reduces neuropsychiatric behaviors by restoring cortical electrophysiological activity in a mouse model of mild traumatic brain injury. Front. Pharmacol 8, 47.
Guida, F., Luongo, L., Boccella, S., Giordano, M.E., Romano, R., Bellini, G., Manzo, I., Furiano, A., Rizzo, A., Imperatore, R., Iannotti, F.A., D'Aniello, E., Piscitelli, F., Sca Rossi, F., Cristino, L., Di Marzo, V., de Novellis, V., Maione, S., et al., 2017b. Palmitoylethanolamide induces microglia changes associated with increased migration and phagocytic activity: involvement of the CB2 receptor. Sci Rep. 7 (1), 375.
Guindon, J., Hohmann, A.G., 2009. The endocannabinoid system and pain. CNS Neurol Disord Drug Targets. 8 (6), 403–421. https://doi.org/10.2174/187152709789824660.
Gundersen, H.J., Jensen, E.B., 1987. The efficiency of systematic sampling in stereology and its prediction. J Microsc 147 (Pt 3), 229–263.
Gustin, S.M., Peck, C.C., Cheney, L.B., Macey, P.M., Murray, G.M., Henderson, L.A., 2012. Pain and plasticity: is chronic pain always associated with somatosensory cortex activity and reorganization. J Neurosci 32 (43), 14874–14884.
Holtmaat, A., Svoboda, K., 2009. Experience-dependent structural synaptic plasticity in the mammalian brain. Nat Rev Neurosci 10 (9), 647–658.
Hurtado-Zavala, J.I., Ramachandran, B., Ahmed, S., Halder, R., Bolleyer, C., Awasthi, A., et al., 2017. TRPV1 regulates excitatory innervation of OLM neurons in the hippocampus. Nat Commun 8, 15878.
Ikonen, S., Riekkinen, P.J., 1999. Effects of apamin on memory processing of hippocampal-lesioned mice. Eur J Pharmacol 382 (3), 151–156.
Imperatore, R., Palomba, L., Morello, G., Spiezio, A.D., Piscitelli, F., Marzo, V.D., Cristino, L., 2016. Formation of OX-1R/CB1R heteromeric complexes in embryonic mouse hypothalamic cells: Effect on intracellular calcium, 2-arachidonoyl-glycerol biosynthesis and ERK phosphorylation. Pharmacol Res 111, 600–609.
Jung, K.M., JinFu, J.R.C., D'Agostino, G., Guijarro, A., Thongkha, D., Avanesian, A., et al., 2012. 2-Arachidonoylglycerol signaling in forebrain regulates systemic energy metabolism. 15 (3), 299–310.
Katona, I., Urbán, G.M., Wallace, M., Ledent, C., Jung, K.M., Piomelli, D., et al., 2006. Molecular composition of the endocannabinoid system at glutamatergic synapses. Journal of Neuroscience 26 (21), 5628–5637.
Kodama, D., Ono, H., Tanabe, M., 2007. Altered hippocampal long-term potentiation after peripheral nerve injury in mice. Eur J Pharmacol 574 (2-3), 127–132.
Koga, K., Shermaine, L., Zhuon, M., et al., 2016. Metabotropic glutamate receptor dependent cortical plasticity in chronic pain. Curr Neuropharmacol 14 (5), 427–434.
Kuner, R., 2015. Spinal excitatory mechanisms of pathological pain. Pain 156 (Suppl. 1), S11–S17.
Kwon, M., Han, J., Kim, U.J., Cha, M., Um, S.W., Bai, S.J., et al., 2017. Inhibition of mammalian target of rapamycin (mTOR) signaling in the insular cortex alleviates neuropathic pain after peripheral nerve injury. Front Mol Neurosci 10, 79.
Lo Verme, J., Fu, J., Astarita, G., La Rana, G., Russo, R., Calignano, A., Piomelli, D., et al., 2005. The nuclear receptor peroxisome proliferator-activated receptor-alpha mediates the anti-inflammatory actions of palmitoylethanolamide. Mol PharmacolJan 67 (1), 15–19.
Lo Verme, J., Russo, R., La Rana, G., Fu, J., Farthing, J., Mattace-Raso, G., et al., 2006. Rapid broad-spectrum analgesia through activation of peroxisome proliferator-activated receptor-alpha. J Pharmacol Exp Ther 319, 1051–1061.
Luongo, L., Maione, S., Di Marzo, V., 2014. Endocannabinoids and neuropathic pain: focus on neuron-glia and endocannabinoid-neurotrophin interactions. Eur J Neurosci. 39 (3), 401–408. https://doi.org/10.1111/ejn.12440.
Lyu, D., Yu, W., Tang, N., Wang, R., Zhao, Z., Xie, F., et al., 2013. The mTOR signaling pathway regulates pain-related synaptic plasticity in rat entorhinal-hippocampal pathways. Mol Pain 9, 64.
Maejima, T., Oka, S., Hashimotodani, Y., Ohno-Shosaku, T., Aiba, A., Wu, D., Waku, K., Sugiura, T., Kano, M., 2005. Synaptically driven endocannabinoid release requires Ca2+-assisted metabotropic glutamate receptor subtype 1 to phospholipase Cbeta4 signaling cascade in the cerebellum. J Neurosci 25 (29), 6826–6835.
Marcaggi, P., Attwell, D., 2005. Endocannabinoid signaling depends on the spatial pattern of synapse activation. Nat Neurosci 8 (6), 776–781.
Marsch, R., Foeller, E., Rammes, G., Bunck, M., Kössl, M., Holsboer, F., et al., 2007. Reduced anxiety, conditioned fear, and hippocampal long-term potentiation in transient receptor potential vanilloid type 1 receptor-deficient mice. J Neurosci 27 (4), 832–839.
McKenna, J.E., Melzack, R., 2001. Blocking NMDA receptors in the hippocampal dentate gyrus with AP5 produces analgesia in the formalin pain test. Exp Neurol 172 (1), 92–99.
Moriarty, O., McGuire, B.E., Finn, D.P., 2011. The effect of pain on cognitive function: a review of clinical and preclinical research. Prog Neurobiol 93 (3), 385–404.
Moriarty, O., Gorman, C.L., McGowan, F., Ford, G.K., Roche, M., Thompson, K., et al., 2016. Impaired recognition memory and cognitive flexibility in the rat L5-L6 spinal nerve ligation model of neuropathic pain. Scand J Pain 10, 61–73.
Musella, A., Fresegna, D., Rizzo, R.F., Gentile, A., Bullitta, S., De Vito, F., Guadalupi, L., Centoze, D., Mandolesi, G., et al., 2017. A novel crosstalk within the endocannabinoid system controls GABA transmission in the striatum. Sci Rep 7, 7363.
Mutso, A.A., Radzicki, D., Baliki, M.N., Huang, L., Banisadr, G., Centeno, M.V., et al., 2012. Abnormalities in hippocampal functioning with persistent pain. J Neurosci 32 (17), 5747–5756.
Ortega-Gutiérrez, S., Molina-Holgado, E., Guaza, C., 2005. Effect of anandamide uptake inhibition in the production of nitric oxide and in the release of cytokines in astrocyte cultures. Glia 52 (2), 163–168.
Palazzo, E., Marabese, I., de Novellis, V., Oliva, P., Rossi, F., Berrino, L., Rossi, F., Maione, S., 2001. Metabotropic and NMDA glutamate receptors participate in the cannabinoid-induced antinociception. Neuropharmacology. 40 (3), 319–326. https://doi.org/10.1016/S0028-3908(00)00160-X.
Palazzo, E., Luongo, L., de Novellis, V., Rossi, F., Maione, S., et al., 2010. The role of cannabinoid receptors in the descending modulation of pain. Pharmaceuticals (Basel) 2661–2673.
Palazzo, E., Luongo, L., Bellini, G., Guida, F., Marabese, I., Boccella, S., Rossi, F., Maione, S., de Novellis, V., et al., 2012. Changes in cannabinoid receptor subtype 1 activity and interaction with metabotropic glutamate subtype 5 receptors in the periaqueductal gray-rostral ventromedial medulla pathway in a rodent neuropathic pain model. CNS Neurol Disord Drug Targets 11 (2), 148–161.
Palazzo, E., Marabese, I., Luongo, L., Boccella, S., Bellini, G., Giordano, M.E., et al., 2013. Effects of a metabotropic glutamate receptor subtype 7 negative allosteric modulator in the periaqueductal grey on pain responses and rostral ventromedial medulla cell activity in rat. Mol Pain 3 (9), 44.
Palazzo, E., Romano, R., Luongo, L., Boccella, S., De Gregorio, D., Giordano, M.E., et al., 2015. MMPIP, an mGluR7-selective negative allosteric modulator, alleviates pain and normalizes affective and cognitive behavior in neuropathic mice. Pain 156 (6), 1060–1073.
Parekh, R., Ascoli, G.A., 2016. Quantitative investigations of axonal and dendritic arbors: development, structure, function and pathology. Neuroscientist 21 (3), 241–254.
Paxinos, G., Franklin, K., 1997. Paxinos and Franklin's the Mouse Brain in Stereotaxic Coordinates, 4th Edition. Academic Press.
Petrosino, S., Iuvone, T., Di Marzo, V., 2010. N-palmitoyl-ethanolamine: biochemistry and new therapeutic opportunities. Biochimie 92 (6), 724–727.
Petrosino, S., Puigdemont, A., della Valle, M.F., Fusco, M., Verdea, R., Allaràa, M., et al., 2016. Adelmidrol increases the endogenous concentrations of palmitoylethanolamide in canine keratinocytes and down-regulates an inflammatory reaction in an in vitro model of contact allergic dermatitis. The Veterinary Journal 207, 85–91.
Piscitelli, F., Carta, G., Bisogno, T., Murru, E., Cordeddu, L., Berge, K., et al., 2011. Effect of dietary krill oil supplementation on the endocannabinoidome of metabolically relevant tissues from high-fat-fed mice. Nutr Metab (Lond) 8 (1), 51.
Rancz, E.A., Häusser, M., 2006. Dendritic calcium spikes are tunable triggers of cannabinoid release and short-term synaptic plasticity in cerebellar Purkinje neurons. J Neurosci 26 (20), 5428–5437.
Ren, W.J., Liu, Y., Zhou, L.J., Li, W., Zhong, Y., Pang, R.P., et al., 2011. Peripheral nerve injury leads to working memory deficits and dysfunction of the hippocampus by upregulation of TNF-α in rodents. Neuropsychopharmacology 36 (5), 979–992.
Rosenzweig, S., Wojtowicz, J.M., 2011. Analyzing dendritic growth in a population of immature neurons in the adult dentate gyrus using laminar quantification of disjointed dendrites. Front Neurosci 5, 34.
Rossi, F., Marabese, I., De Chiaro, M., Boccella, S., Luongo, L., Guida, F., et al., 2014. Dorsal striatum metabotropic glutamate receptor 8 affects nocifensive responses and rostral ventromedial medulla cell activity in neuropathic pain conditions. J Neurophysiol 111 (11), 2196–2209.
Ryberg, E., Larsson, N., Sjögren, S., Hjorth, S., Hermansson, N.O., et al., 2007. The orphan receptor GPR55 is a novel cannabinoid receptor. Br J Pharmacol 152 (7), 1092–1101.
Ryskalin, L., Lazzeri, G., Flaibani, M., Biagioni, F., Gambardella, S., Frati, A., Fornai, F., et al., 2017. mTOR-dependent cell proliferation in the brain. Biomed Res Int 7082696.
Saxe, M.D., Battaglia, F., Wang, J.-W., Malleret, G., David, D.J., Monckton, J.E., Garcia, A. Denise R., Sofroniew, M.V., Kandel Eric, R., Santarelli, L., Hen, R., Drew Michael, R., et al., 2006. Ablation of hippocampal neurogenesis impairs contextual fear conditioning and synaptic plasticity in the dentate gyrus. Proc Natl Acad Sci U S A 103 (46), 17501–17506.
Schoepp DD, Janeb DE, Monna JA. Pharmacological agents acting at subtypes of metabotropic glutamate receptors. Neuropharmacology 38(10) 1431-1476
Seralynne, D.V., 2013. Dismantling the Papez circuit for memory in rats. eLife 2, e00736.
Sestito, S., Rodrigo, Trindade, B., Lucas, de Souza, G., Rodrigo, Kerbauy, Lucila, Iyomasa, M., Melina, Rosa, L.N.M., Maria, 2010. Effect of isolation rearing on the expression of AMPA glutamate receptors in the hippocampal formation. Journal of Psychopharmacology 25, 1720–1729.
Smith, J.S., Rajagopal, S., 2016. The β-arrestins: multifunctional regulators of G protein-coupled receptors. J Biol Chem 291 (17), 8969–8977 Review.
Suardíaz, M., Estivill-Torrús, G., Goicoechea, C., Bilbao, A., Rodríguez de Fonseca, F., 2007. Analgesic properties of oleoylethanolamide (OEA) in visceral and inflammatory pain. Pain 133 (1-3), 99–110.
Thompson, J.M., Neugebauer, V., 2017. Amygdala plasticity and pain. Pain Res Manag. 2017, 8296501.
Truini, A., Garcia-Larrea, L., Cruccu, G., et al., 2013. Reappraising neuropathic pain in humans—how symptoms help disclose mechanisms. Nat Rev Neurol 9 (10), 572–582.
Van der Staay, F.J., Fanelli, R.J., Blokland, A., Schmidt, B., 2000. Behavioral effects of apamin, a selective inhibitor of the SK(Ca)- channel, in mice and rats. Neuroscience and biobehavioral reviews 23, 1087–1110.
Violin, J.D., Ren, X.R., Lefkowitz, R.J., 2006. G-protein-coupled receptor kinase specificity for beta-arrestin recruitment to the beta2-adrenergic receptor revealed by fluorescence resonance energy transfer. J Biol Chem 281 (29), 20577–20588.

Walker, A.K., Kavelaars, A., Heijnen, C.J., Dantzer, R., 2013. Neuroinflammation and comorbidity of pain and depression. Pharmacol Rev 66 (1), 80–101.
Wang, S.J.N., 2003. Cannabinoid CB1 receptor-mediated inhibition of glutamate release from rat hippocampal synaptosomes. Eur J Pharmacol 469 (1-3), 47–55.
Wang, W., Trieu, B.H., Palmer, L.C., Jia, Y., Pham, D.T., Jung, K.M., Karsten, C.A., Merrill, C.B., Mackie, K., Gall, C.M., Piomelli, D., Lynch, G., et al., 2016. A primary cortical input to hippocampus expresses a pathway-specific and endocannabinoid-dependent form of long-term potentiation. eNeuro 3 (4).
Wang, W., Jia, Y., Pham, D.T., Palmer, L.C., Jung, K.M., Cox, C.D., Rumbaugh, G., Piomelli, D., Gall, C.M., Lynch, G., Jul 1, 2018. Atypical endocannabinoid signaling initiates a new form of memory-related plasticity at a cortical input to Hippocampus. Cereb Cortex 28 (7), 2253–2266.
Wieronska, J.M., Pilc, A., 2009. Metabotropic glutamate receptors in the tripartite synapse as a target for new psychotropic drugs. Neurochem. Int 85–97.
Yalcin, I., Bohren, Y., Waltisperger, E., Sage-Ciocca, D., Yin, J.C., Freund-Mercier, M.J., et al., 2011. A time-dependent history of mood disorders in a murine model of neuropathic pain. Biol Psychiatry 70 (10), 946–953.
Zhang, Y., Liu, F.Y., Liao, F.F., Wan, Y., Yi, M., 2014. Exacerbation of tonic but not phasic pain by entorhinal cortex lesions. Neurosci Lett 581, 137–142.
Zschenderlein, C., Gebhardt, C., von Bohlen Und Halbach, O., Kulisch, C., Albrecht, D., 2011. Capsaicin-induced changes in LTP in the lateral amygdala are mediated by TRPV1. PLoS One 6 (1), e16116.